Rate-dependent viscoplastic modeling and experimental validation of woven glass/epoxy composite materials

Ehsan Shafiei[a], Mahdi Saed Kiasat[a], Ever.J Barbero[b*]

[a] Department of Maritime Engineering, Amirkabir University of Technology, No. 350, Hafez Ave, Valiasr Square, Tehran, Iran.

[b] Department of Continuum Mechanics and Structural Analysis, Universidad Carlos III de Madrid, Madrid, Spain

[*]Corresponding Author:

DOI: https://doi.org/10.1016/j.compositesb.2021.108827

Final Revision

Abstract

The rate-dependent behavior of woven fabric (WF) composite with material nonlinearity and 3D geometrical nonuniformity are predicted using a proposed micro-meso-scale (MMS) model. The viscoelastic fiber and viscoplastic matrix are combined to obtain the properties of viscoplastic composite tows. Applying geometrical properties of WF and considering different local position and orientation of tows, the orthotropic viscoplastic behavior of WF composite is obtained. A progressive damage model is developed to consider damage modes in the composite tows. The stresses are redistributed over the intact regions according to the occurrence of the specific damage modes. Experimental rate-dependent tests are carried out on the epoxy matrix and unidirectional composite to measure the model constants. The rate dependency of the mechanical properties and nonlinearity of the stress-strain curves of the WF composite are then predicted and compared to additional experimental tests on the WF composite.

Keywords

Elastic-viscoplastic material; Constitutive behavior; Analytic functions; Strengthening and mechanisms; Mechanical testing

1. Introduction

Woven fabric (WF) composites have benefits such as damage tolerance with application to marine, aerospace, and automotive industry. The WF laminates show nonlinear stress-strain curves due to the irreversible inelastic behavior of composite constituents and three-dimensional fabric structure. In addition, the initial mechanical properties and ultimate strength are loading-rate dependent. Accurate prediction of the mechanical response of the WF composites are addressed here by considering four aspects, material nonlinearity, damage, rate-dependency, and WF internal geometry.

The material nonlinear behavior of the WF composite that is due to the inelastic behavior of the matrix material has been studied by proposing various models to calculate plastic and viscoplastic deformations. Chung, Ogihara and Thiruppukuzhi [1-3] proposed potential functions

in terms of in-plane stresses to derive the plastic strain of the WF laminates and predict the nonlinear stress-strain curve. Marguet et al. [4] and Hochard et al. [5] proposed a potential function based on the in-plane shear stress to derive the plastic deformation of the WF composite. They suggested that in-plane shear stress is the effective parameter on the plastic behavior of the WF laminate. These macro-scale potential functions were used to calculate the global nonlinearity of the WF composite and did not take into account the share of matrix material on the nonlinear behavior of the WF composite. Huang [6] developed a micromechanical model that can take into account the effect of plastic behavior of the matrix material on the mechanical properties of unidirectional (UD) composite. Bai et al. [7], Goldberg and Stouffer [8], and Hsu et al. [9] proposed different forms of potential function based on the hydrostatic stress and second invariant of deviatoric stress to derive the viscoplastic behavior of matrix material. Shafiei and Kiasat [10] proposed a potential function based on the first invariant of stress, second and third invariants of deviatoric stress to derive the viscoplastic behavior of polymeric matrix. The constitutive equation considered the effects of hydrostatic and distortion stresses as well as the effect of loading angle.

The loading-rate effects on the mechanical behaviors of the WF composite have been studied by means of experimental works. Lu et al. [11] demonstrated that increasing applied strain rate from 10^{-3} to 10^{3} s^{-1} on plain woven carbon/epoxy laminates result in an increase about 8.6% and 23% in the tensile initial modulus and strength [11]. Li et al. [12] showed that high strain rate from 1281 to 2310 s^{-1} causes about 63% increase of ultimate strength of plain woven carbon/epoxy laminates. Chen et al. [13] illustrated that the linear stress-strain curve of woven carbon/epoxy composite at low strain rate of 10^{-3} s^{-1} changes to a nonlinear curve after increasing strain rate up to 1.8×10^{2} s^{-1}. Chung and Ryou [1] performed rate-dependent tensile tests on woven glass/epoxy fabric from 5×10^{-6} to 5×10^{-2} s^{-1} strain rates and data shows high rate-dependency of initial modulus which increases about 20%. On the other hand, Fitoussi et al [14] found that tensile modulus of woven carbon-epoxy laminates had no strain-rate dependency but increasing the strain rate from 0.5 to 60 s^{-1} increases the tensile strength about 24%.

Analytical meso-scale based methods have been chosen by researchers in the literature [6, 15-17] to describe the behavior of the WF laminate, where the material and geometrical description of the WF laminate were performed by considering a representative volume element (RVE) which is selected over the WF laminate. The three-dimensional RVE contains effective parts of the interlaced warp and fill composite tows. Kwon and Cho [16] modeled the composite tows with rectangular cross-section and ignored the undulation of tows over each other. Scida et al. [17] modeled composite tows considering their elliptical cross-section and undulation and used trigonometric functions to calculate the elastic behavior of WF laminate. Huang [6] and Adumitroaie and Barbero [15] took into account the gap between adjacent tows in addition to the undulation and elliptical cross-section of composite tows.

In this study, the nonlinear rate-dependent mechanical behavior of the WF composite is predicted using a new micro-meso-scale (MMS) model. The model considers the combined effects of rate-dependent properties, viscoelastic glass fibers, viscoplastic polymeric matrix, damage

propagation, and 3D nonuniform geometry of the WF on the final nonlinear rate-dependent behavior of the WF composite.

In this study, the micro- and meso-scale (MMS) models consider both the material nonlinearity and geometrical properties under rate-dependent loadings. The fiber and matrix with viscoelastic and viscoplastic behavior are combined in the micro-scale model to build UD composite tow with viscoplastic behavior. The interplay between the fiber rate-dependency elasticity and matrix rate-dependent viscoplastic behavior are implemented in the micro-scale model. Furthermore, the sinusoidal tow geometry and stacking sequence in the meso-scale model result in a WF composite with anisotropic viscoplastic behavior. At each differential step, the viscoplasticity of matrix and viscoelasticity of the fiber are updated, and consequently, the viscoplasticity of the composite tows and the WF composite are also updated.

Furthermore, a strain-rate-dependent progressive damage model is developed to enhance the prediction of the stress-strain curves of the WF composite based on the viscoplastic behavior of sub-elements, composite tow, and matrix. Once the modes of damage are detected and failures occur in the specific directions of the sub-elements, the relevant stiffness matrices of sub-element are degraded, then the stiffness matrix of the RVE is updated and the stresses are redistributed over the intact regions. To derive the viscoplastic model constants, a series of experimental tests are carried out on the epoxy matrix and UD glass/epoxy composite at different strain rates. The MMS model is verified with good agreement by tensile tests performed on plain WF glass/epoxy composite at various strain-rates.

While [15, 17, 18] describe a model to compute the elastic properties and strength of a fabric reinforced lamina, their analysis is limited to elastic materials. In this work, the model is extended to include rate-dependent fibers, rate-dependent viscoplastic matrix, and their effects on the final response of the WF composite. Furthermore, novel experimental data are presented. First, rate-dependent experimental data of unidirectional lamina is presented and used to calculate the rate-dependent properties of the fiber. Second, novel experimental data of Epoxy matrix is presented and used to calculate the matrix rate-dependent viscoplastic properties. Third, novel data is presented to study the rate-dependent viscoplastic response of woven fabric reinforced laminates and used to verify the numerical model. Fourth, in the MMS model, the effects of material properties and geometrical features on the rate-dependent viscoplastic behavior of the WF composite are addressed separately.

2. Viscoplastic rate-dependent MMS Mechanical Modeling

In the MMS analysis, the matrix and fiber are considered as viscoplastic and viscoelastic materials, respectively. The consequent viscoplastic composite tows from micromechanical modeling and geometrical properties of woven fabric are used in the developed meso-scale model to obtain a macro-scale WF composite with anisotropic viscoplastic behavior is obtained.

2.1. Rate-dependent micro-scale modeling

2.1.1. Elastic relations of UD composite tow

Micromechanics is the study of composite materials by considering the interaction of its constituent, fiber and matrix. In the micromechanics, the effective properties and response of the composite are calculated based on the properties and response of the constituents. Huang [6] proposed a micromechanical model to predict the effective properties and response of polymeric matrix UD composites under static loading. Characteristic of this model is that the stresses in the constituents of the composite are amended by a bridging matrix. The bridging matrix depends on the elastic and tangent moduli of the constituents. This approach is used here to develop a micromechanical model to predict rate-dependent behavior of composite tows.

The bridging matrix $[P_{ij}]$ maps the average stress in the fiber $\{\sigma_i^f\}$ to the average stress in the matrix $\{\sigma_i^m\}$ as follows [6]

$$\{\sigma_i^m\} = [P_{ij}]\{\sigma_i^f\}, \quad i, j = 1, ..., 6 \tag{1}$$

The general form of the bridging matrix with nonzero elements is defined as follows [6]

$$[P_{ij}] = \begin{bmatrix} a_{11} & a_{12} & a_{13} & 0 & 0 & 0 \\ 0 & a_{22} & 0 & 0 & 0 & 0 \\ 0 & 0 & a_{33} & 0 & 0 & 0 \\ 0 & 0 & 0 & a_{44} & 0 & 0 \\ 0 & 0 & 0 & 0 & a_{55} & 0 \\ 0 & 0 & 0 & 0 & 0 & a_{66} \end{bmatrix} \tag{2}$$

$$\begin{aligned} a_{11} &= \frac{E_m^T}{E_{fa}} \\ a_{22} = a_{33} = a_{44} &= \beta + \frac{(1-\beta)E_m^T}{E_{ft}}, \quad 0 < \beta < 1 \\ a_{55} = a_{66} &= \alpha + \frac{(1-\alpha)G_m^T}{G_{fa}}, \quad 0 < \alpha < 1 \\ a_{12} = a_{13} &= \frac{(S_{12}^f - S_{12}^m)(a_{11} - a_{22})}{(S_{11}^f - S_{11}^m)} \end{aligned} \tag{3}$$

In Eqs. (2) and (3), G_m^T and E_m^T are the shear and Young's tangent modulus of the matrix material that are tangent to the stress-strain curve at each time step. E_{fa}, E_{ft} and G_{fa} are the axial, transverse, and axial shear moduli of the fiber, respectively. The model parameters α and β are used to adjust the model with experimental results of UD composite, as explained in [6].

Assuming that the out-of-plane shear responses are the same, then $a_{55} = a_{66}$. Experiments have been shown [6] that the transverse normal stresses of a UD composite are directly comparable to each other, $\sigma_2^m = a_{22}\sigma_2^f$, $\sigma_3^m = a_{33}\sigma_3^f$, while the longitudinal stress can be assumed to correlate by three normal stress components, $\sigma_1^m = a_{11}\sigma_1^f + a_{12}\sigma_2^f + a_{13}\sigma_3^f$. Therefore, the bridging matrix is not symmetric but that does not affect the symmetry of the fiber and matrix stress, which in (1) are written in contracted notation, thus assuming symmetry of stress. In Eq. (3), S_{ij}^f and S_{ij}^m $(i, j = 1,...,6)$ are the elements of compliance matrices of fiber $[S_{ij}^f]$ and matrix $[S_{ij}^m]$ respectively. Parameters α and β in the bridging parameters control the influence of the transverse and shear components of fiber stress, respectively, on the like components of matrix stress. These parameters are adjusted with experimental data as per [6].

The relations of average stress $\{\sigma_i\}$ and strain $\{\varepsilon_i\}$ of the UD composite tow in terms of average stress and strain of the fibers and matrix material are as

$$\{\sigma_i\} = v_f\{\sigma_i^f\} + v_m\{\sigma_i^m\} \tag{4}$$

$$\{\varepsilon_i\} = v_f\{\varepsilon_i^f\} + v_m\{\varepsilon_i^m\} \tag{5}$$

$$\{\varepsilon_i\} = [S_{ij}]\{\sigma_j\} \quad i, j = 1,...,6 \tag{6}$$

For the tow, v_f and v_m are tow's fiber and matrix volume fractions, in contrast to the overall volume fraction in the meso-scale, Eq. (9.7) in [18]. The total strain in representative volume element of UD composite is summation of volume-average strain of fiber, matrix, and voids. However, the void fraction is less than 1% in composite with acceptable quality. So that, the total strain is summation of volume-average strain of fiber and matrix [19]. In Eq. (6), $[S_{ij}]$ is the compliance matrix of the UD composite tow. The stress and strain components in the fibers and the matrix are calculated in terms of compliance matrices

$$\begin{aligned} \{\varepsilon_i^f\} &= [S_{ij}^f]\{\sigma_j^f\} \\ \{\varepsilon_i^m\} &= [S_{ij}^m]\{\sigma_j^m\} \end{aligned} \tag{7}$$

By substituting Eq. (1) into Eq. (4) and using Eqs. (5)-(7), the compliance matrix of the composite tow in the local coordinate system is obtained as a function of the mechanical properties of the fibers and matrix materials

$$[S_{ij}] = (v_f[S_{ij}^f] + v_m[S_{ij}^m][P_{ij}])(v_f[I_{ij}] + v_m[P_{ij}])^{-1} \tag{8}$$

By means of Eqs. (7) and (1) into Eq. (5), the following equations are obtained to express the strain components of fibers $\{\varepsilon_i^f\}$ and matrix material $\{\varepsilon_i^m\}$ in terms of total strain of the composite tow $\{\varepsilon_j\}$

$$\{\varepsilon_i^f\} = [S_{ij}^f](v_f[S_{ij}^f] + v_m[S_{ij}^m][P_{ij}])^{-1}\{\varepsilon_j\} \tag{9}$$

$$\{\varepsilon_i^m\} = [S_{ij}^m][P_{ij}](v_f[S_{ij}^f] + v_m[S_{ij}^m][P_{ij}])^{-1}\{\varepsilon_j\} \tag{10}$$

2.1.2. Viscoplastic relations of UD composite tow

Viscoplastic relations for fibrous composites are based on the nonlinear rate-dependent mechanical behavior of composite constituents which appear in $[P_{ij}]$ and $[S_{ij}]$ matrices. In this method, the strains in constitutive equations of composite are divided into the elastic and inelastic strains. The polymeric matrix material is assumed to have viscoplastic properties. On the other hand, fibers are assumed to have a rate-dependent elastic behavior, which is acceptable for a wide range of structural fibers such as glass [20]. On this basis, the total strain components of composite $\{\varepsilon_i\}$ are divided into an elastic $\{\varepsilon_i\}^E$ and inelastic $\{\varepsilon_i\}^I$ parts

$$\{\varepsilon_i\} = \{\varepsilon_i\}^E + \{\varepsilon_i\}^I \tag{11}$$

The elastic and inelastic strain components are defined based on the elastic terms of fiber, elastic and inelastic terms of matrix, and furthermore their time derivatives

$$\{\varepsilon_i\}^E = v_f\{\varepsilon_i^f\}^E + v_m\{\varepsilon_i^m\}^E, \quad \{\varepsilon_i\}^I = v_m\{\varepsilon_i^m\}^I \tag{12}$$

$$\{\dot{\varepsilon}_i\}^E = v_f\{\dot{\varepsilon}_i^f\}^E + v_m\{\dot{\varepsilon}_i^m\}^E, \quad \{\dot{\varepsilon}_i\}^I = v_m\{\dot{\varepsilon}_i^m\}^I \tag{13}$$

The strain rate components of fiber $\{\dot{\varepsilon}_i^f\}$ and matrix $\{\dot{\varepsilon}_i^m\}$ are time derivatives of Eqs. (9) and (10). The mechanical properties of materials in Eq. (8) are functions of strain rate and using the chain derivative, the time derivative of the mechanical properties can be calculated. For instance, the time derivative of the elements of compliance matrix is $dS_{ij}/dt = (dS_{ij}/d\dot{\varepsilon})(d\dot{\varepsilon}/dt)$. At constant strain-rate loading $\dot{\varepsilon} = c$, the time derivative of the mechanical properties is zero $dS_{ij}/dt = 0$. In addition, for each arbitrary load condition, the strain rate at each differential step can be assumed constant. Thus, the time derivative of the mechanical properties is zero during a differential step, and the strain rate components of fiber and matrix are

$$\{\dot{\varepsilon}_i^f\} = [S_{ij}^f](v_f[S_{ij}^f] + v_m[S_{ij}^m][P_{ij}])^{-1}\{\dot{\varepsilon}_j\} \tag{14}$$

$$\{\dot{\varepsilon}_i^m\} = [S_{ij}^m][P_{ij}](v_f[S_{ij}^f] + v_m[S_{ij}^m][P_{ij}])^{-1}\{\dot{\varepsilon}_j\} \tag{15}$$

In the proposed micromechanics model, the elements of Eqs. (1) and (8) are function of strain rate and should be rewritten as

$$\left\{d\sigma_j^m(\dot{\varepsilon})\right\} = \left[P_{ij}(\dot{\varepsilon})\right]\left\{d\sigma_i^f(\dot{\varepsilon})\right\} \tag{16}$$

$$[S_{ij}(\dot{\varepsilon})] = (v_f[S_{ij}^f(\dot{\varepsilon})] + v_m[S_{ij}^m(\dot{\varepsilon})][P_{ij}(\dot{\varepsilon})])(v_f[I_{ij}] + v_m[P_{ij}(\dot{\varepsilon})])^{-1} \tag{17}$$

Eq. (15) indicates the share of strain rate in the matrix material from which the inelastic strain rate should be reduced. Further, the inelastic strain rate of matrix $\dot{\varepsilon}_{ij}^{m^I}$ is obtained through the viscoplastic constitutive equation [10] as follows

$$\dot{\varepsilon}_{ij}^{m^I} = \frac{2D_0}{3\sigma_e^2}\exp\left[-\frac{1}{2}\left(\frac{Z}{\sigma_e}\right)^{2n}\right]\left[\frac{3}{2}\sigma_{ij}^d\sqrt{J_2} - C(t_{ij}' + 3I_1^2\delta_{ij})\right] \tag{18}$$

The inelastic strain rate of matrix, Eq. (18), is derived from the following potential function, Eq. (19), by means of an associated flow rule.

$$f = J_2^{3/2} - C(J_3 + I_1^3) \tag{19}$$

The inelastic strain rate of matrix is a function of second J_2 and third J_3 invariant of deviatoric stress tensor, first invariant of stress tensor I_1, effective stress σ_e, and model parameters *Z*, *C*, D_0 and *n*. t'_{ij} is the derivative of J_3 respect to deviatoric stress σ^d_{ij}. C is determine by preserving the convexity of the potential function, Eq. (19), n and Z control the rate dependency and hardening of the polymeric matrix material, and D_0 has a constant value of 10^6. Details on how to obtain the model parameters and extraction of Eq. (18) are explained in [10].

$$t'_{ij} = \frac{\partial J_3}{\partial \sigma^d_{ij}} = \sigma^d_{ik}\sigma^d_{kj} - \frac{2}{3} J_2 \delta_{ij} \tag{20}$$

In Eq. (18), J_2, J_3 and I_1 represent the effects of distortion, load angle and hydrostatic stress on the viscoplastic deformation.

2.2. Rate-dependent meso-scale Modeling

2.2.1. Representative Volume Element

The weave pattern is the main characteristic of woven fabrics that imparts the benefits in the mechanical properties and fabrication with WF. Inherent undulation of the warp and fill tows due to the interlacing and weaving of tows in the fabric induces curvatures of the warp and fill composite tows on the yz and xz planes, which behave like off-axis composites, Fig. 1. From a geometrical viewpoint, all variable geometric components of the woven fabric, such as lenticular-like cross-section of tows, undulation, and the gap between adjacent tows, lead to a variable stiffness field. Due to the geometry and stacking sequence of warp and fill composite tows in the WF composite, Fig. 1, the stiffness changes across the surface (x, y positions) of the WF layer.

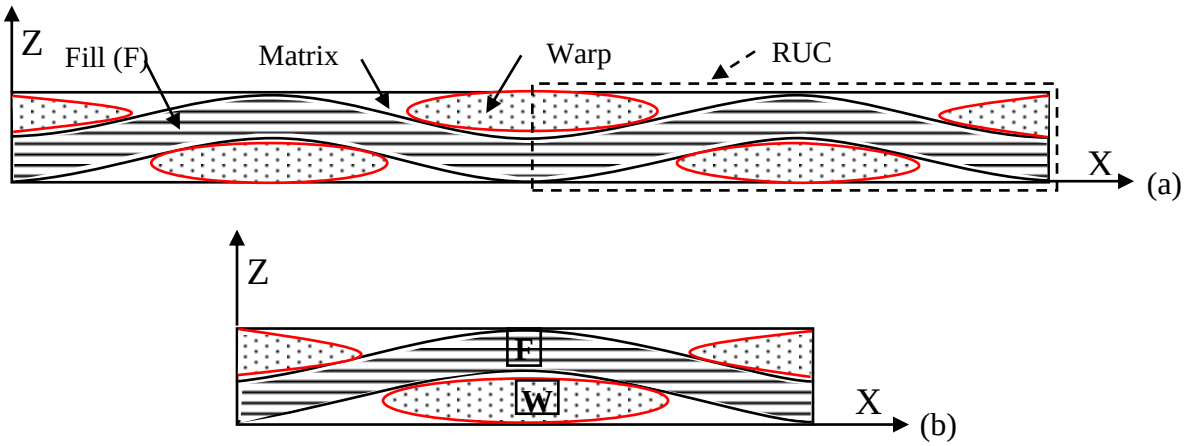

Fig. 1. (a) Cross-section of a single WF layer, (b) selected RUC of a WF layer

Analytical modeling of the mechanical behavior of the WF composites considering varying mechanical and geometrical considerations is performed by defining a three-dimensional RVE consisting of interweaved composites of warp and fill tows. To create an RVE, a repetitive unit cell (RUC) of WF composite is considered, which has periodic properties and expresses the mechanical properties of the whole composite, Fig. 1. The two symmetrical planes of RUC of plain WF structure allows further reduction of the size required for analysis, to be a quarter RUC, Fig. 2(a). In addition, the quarter RUC with anti-symmetry conditions allows the selection of RVE, Fig. 2(b), which is 1/16 RUC and still represents the mechanical behavior of the WF layer.

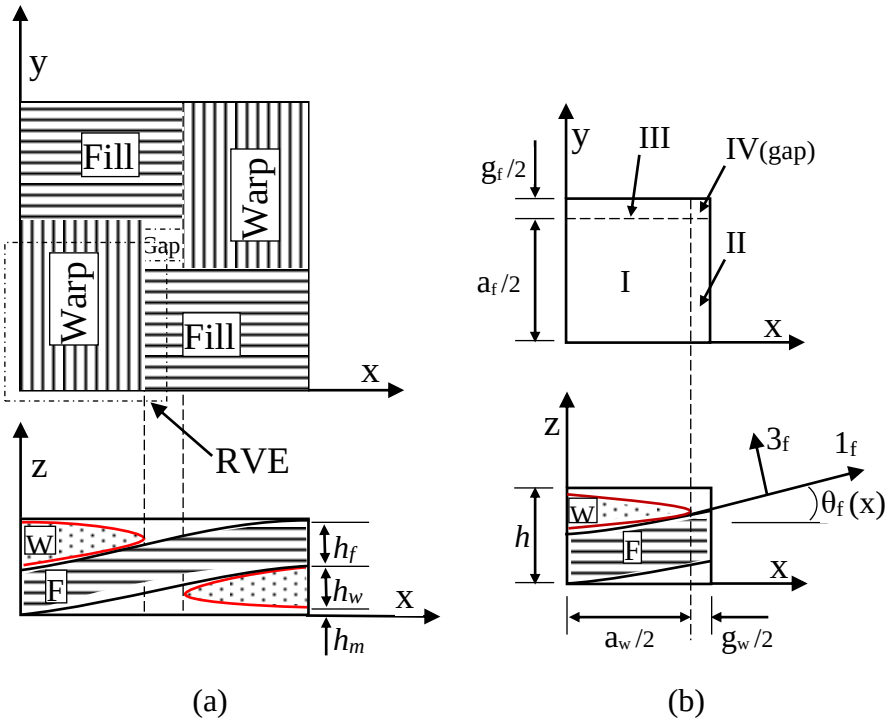

Fig. 2. Top and side views of (a) one quarter of an RUC, and (b) an RVE with details.

The following equations provide a three-dimensional definition of RVE. The input parameters, presented in Fig. 2, include the thickness h and width a of the tow, and the gap g between the contiguous tows. Subscripts w, f and m represent the warp, fill and matrix elements, respectively. In the RVE geometric description, the formulations of the surfaces of the warp and fill composite tows are carried out to calculate the local undulation θ and the occupied volume of the warp and fill composite tows V. The upper and lower boundary surfaces, z_w^{upper}, z_w^{lower}, z_f^{upper} and z_f^{lower}, of the undulated composites of warp and fill tows are defined as follows [15]

$$z_w^{upper}(x,y) = -\frac{h_w}{2}\cos\frac{\pi y}{a_f + g_f} + \frac{1}{2}\left|h_w \cos\frac{\pi x}{a_w}\right| \quad \text{for } x \in [0, \frac{a_w}{2}] \tag{21}$$

$$z_w^{lower}(x,y) = -\frac{h_w}{2}\cos\frac{\pi y}{a_f+g_f} - \frac{1}{2}\left|h_w\cos\frac{\pi x}{a_w}\right| \text{ for } x\in[0,\frac{a_w}{2}] \tag{22}$$

$$z_f^{upper}(x,y) = -\frac{h_f}{2}\cos\frac{\pi x}{a_w+g_w} + \frac{1}{2}\left|h_f\cos\frac{\pi y}{a_f}\right| \text{ for } y\in[0,\frac{a_f}{2}] \tag{23}$$

$$z_f^{lower}(x,y) = -\frac{h_f}{2}\cos\frac{\pi x}{a_w+g_w} - \frac{1}{2}\left|h_f\cos\frac{\pi y}{a_f}\right| \text{ for } y\in[0,\frac{a_f}{2}] \tag{24}$$

In the above equations, the first and second terms indicate the height of the middle surface and half the thickness of the composite tow's cross-section. Using Eqs. (21)-(24), the undulation angle of the warp θ_w and fill θ_f tows, which are the local off-axis angles, are determined as follows

$$\theta_w(y) = \left|\arctan\left(\frac{d}{dy}z_w(y)\right)\right| \tag{25}$$

$$\theta_f(x) = \left|\arctan\left(\frac{d}{dx}z_f(x)\right)\right| \tag{26}$$

The volume occupied by the warp V_w and fill V_f composite tows inside the RVE are obtained by multiplying the cross-sectional area by the undulated length

$$V_w = \int_0^{\frac{a_f+g_f}{2}}\int_0^{\frac{a_w+g_w}{2}} h_w\sqrt{1+\left(\frac{d}{dy}z_w(y)\right)^2}\cos\frac{\pi x}{a_w}dxdy \tag{27}$$

$$V_f = \int_0^{\frac{a_w+g_w}{2}}\int_0^{\frac{a_f+g_f}{2}} h_f\sqrt{1+\left(\frac{d}{dx}z_f(x)\right)^2}\cos\frac{\pi y}{a_f}dydx \tag{28}$$

For the case of similar fiber volume fraction of the warp and fill composite tows v_f, their volume fraction is calculated as follows by the overall fiber volume fraction of the WF composite v_f^c, the latter is determined experimentally, and values are presented in Table 2.

$$v_f = v_f^c\frac{h(a_w+g_w)(a_f+g_f)}{4(V_w+V_f)}, \quad v_m = 1-v_f, \quad h = h_w+h_f+h_m \tag{29}$$

2.2.2. Rate-dependent stiffness matrices of the WF composite

At the meso-scale analysis, the warp and fill tows are regarded as off-axis UD composites governed by equations in section 2.1. The viscoplastic behavior of the WF composite is obtained through Eqs. (30)-(33) based on the viscoplastic properties of the composite tows and their geometrical characteristics such as elliptical cross-section and undulation, and geometrical specifications of RVE in the meso-scale. In order to optimize the computational effort, the RVE is divided into four regions with different stacking sequences [15], regions I to IV in Fig. 2(b).

The stacking of the WF layers from bottom to top in regions I, II, III and IV are matrix/fill/warp/matrix, matrix/fill/matrix, matrix/warp/matrix, and pure resin, respectively. Each of the four regions is interpreted as a multi-layered composite with strain-rate-dependent stiffness matrix $[A_{ij}]$. The extensional stiffness matrix $[A_{ij}]$ is a function of (x,y) coordinates of the RVE surface due to the undulation of the warp and fill composite tows. It can be written in terms of the through the thickness integration of the transformed stiffness matrices $[C'_{ij}(x,y)]$ of the warp, fill, and matrix layers as follows

$$[A_{ij}(\dot{\varepsilon},x,y)]=\int_{-h/2}^{h/2}[C'_{ij}(\dot{\varepsilon},x,y)]dz \quad i,j=1,...,6 \tag{30}$$

where $[C'_{ij}]=[S'_{ij}]^{-1}$, the transformed compliance matrix $[S'_{ij}]^{-1}$ is obtained from Eq. (31), and the compliance matrix $[S_{ij}]$ for the matrix and composite tow are obtained from Eq. (17)

$$[S'_{ij}(\dot{\varepsilon},x,y)]=[T_{ij}(x,y)]^T[S_{ij}(\dot{\varepsilon},x,y)][T_{ij}(x,y)] \tag{31}$$

The warp $[T_{ij}(x,y)]_w$ and fill $[T_{ij}(x,y)]_f$ transformation matrices are described in terms of sine and cosine of the undulated angle of warp $\theta_w(y)$ and fill $\theta_f(x)$ composite tows. The strain-rate dependent stiffness matrix of the RVE is obtained through a dual integral averaging process over the four regions of the RVE surface, as follows

$$[\bar{A}_{ij}(\dot{\varepsilon})]=\frac{4}{(a_w+g_w)(a_f+g_f)}\times\int_0^{(a_w+g_w)/2}\int_0^{(a_f+g_f)/2}[A_{ij}(\dot{\varepsilon},x,y)]dxdy \tag{32}$$

Based on the elements of the stiffness matrix $[\bar{A}_{ij}(\dot{\varepsilon})]$, the rate-dependent tensile moduli $E_x(\dot{\varepsilon}), E_y(\dot{\varepsilon})$, shear modulus $G_{xy}(\dot{\varepsilon})$, and the poison's ratio v_{xy} of the WF composite are obtained as follows

$$\begin{aligned} &E_x(\dot{\varepsilon})=\frac{\bar{A}_{11}(\dot{\varepsilon})\bar{A}_{22}(\dot{\varepsilon})-\bar{A}_{12}^2(\dot{\varepsilon})}{h\bar{A}_{22}(\dot{\varepsilon})},\ E_y(\dot{\varepsilon})=\frac{\bar{A}_{11}(\dot{\varepsilon})\bar{A}_{22}(\dot{\varepsilon})-\bar{A}_{12}^2(\dot{\varepsilon})}{h\bar{A}_{11}(\dot{\varepsilon})},\\ &G_{xy}(\dot{\varepsilon})=\frac{\bar{A}_{66}(\dot{\varepsilon})}{h},\ v_{xy}=\frac{\bar{A}_{12}(\dot{\varepsilon})}{\bar{A}_{22}(\dot{\varepsilon})} \end{aligned} \tag{33}$$

In the experimental tests, the mechanical properties of materials such as modulus and strength are determined at specific point-wise strain rates. The following logarithmic model is used to fit the experimental results, so that the modulus and strength of the material at other strain rates can be obtained as well.

$$A(\dot{\varepsilon})=A_0[1+B\ln(\frac{\dot{\varepsilon}}{\dot{\varepsilon}_0})] \tag{34}$$

where A is the mechanical property (modulus or strength), A_0 is the value of A at the reference strain rate $\dot{\varepsilon}_0$, and B is a constant that is determined by curve fitting.

3. Strength and failure criteria

Based on the failure propagation method at the onset of material failure, the stiffness matrix is degraded using an incremental-iterative scheme and the load is redistributed over the intact regions. To obtain a good approximation to the strength, the RVE in Fig. 2 is divided into $N \times M$ elements along *x* and *y* directions, Fig. 3. The strength is calculated using the average stresses in the sub-elements, the warp and fill composite tows and the pure matrix. According to the iso-strain assumption, the applied in-plane strain tensor $\{\varepsilon_x, \varepsilon_y, \varepsilon_{xy}\}^T$ on the WF composite is uniformly transmitted to the elements [15, 18, 21]. Using the local transformation matrices of the sub-elements, the local stress values are calculated. The element-based strength analysis and progressive failure are performed to degrade the stiffness matrix at the occurrence of single or simultaneous multiple damage modes.

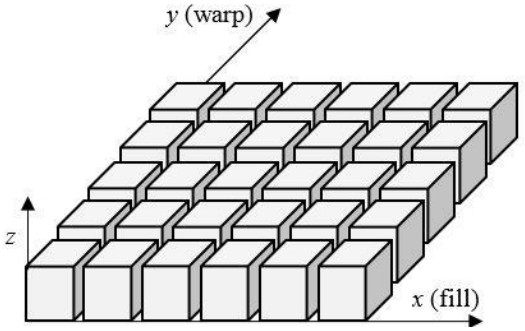

Fig. 3. Discretization of the RVE into elements

The rate-dependent progressive damage model predicts the strength of the WF composite by predicting the onset of failure of the sub-elements and applies their effects on the strength of the elements and the whole WF composite. According to experimental results, there is no sudden failure in the WF composite, but some composite elements break down sooner than others. The proposed rate-dependent failure criterion is an extension of the Hashin failure criterion [22] with strain-rate-dependent mechanical properties used at each time step. Failure of composite tows and pure matrix are predicted using the proposed rate-dependent criterion.

3.1. Rate-dependent failure criteria

3.1.1. Rate-dependent longitudinal tensile mode

"Longitudinal tensile mode" means traction failure along the fiber direction of a tow. Rate-dependent tensile failure subjected to the tensile stress $\sigma_{11}(\dot{\varepsilon}^{(n)}) > 0$, is predicted by

$$I_1 = \left(\frac{\sigma_{11}(\dot{\varepsilon}^{(n)})}{F_{1t}(\dot{\varepsilon}^{(n)})}\right)^2 + \left(\frac{\tau_{12}(\dot{\varepsilon}^{(n)})}{F_6(\dot{\varepsilon}^{(n)})}\right)^2 + \left(\frac{\tau_{23}(\dot{\varepsilon}^{(n)})}{F_4(\dot{\varepsilon}^{(n)})}\right)^2 \geq 1 \tag{35}$$

This equation states that when the stresses $\sigma_{11}(\dot{\varepsilon}^{(n)})$, $\tau_{12}(\dot{\varepsilon}^{(n)})$ and $\tau_{23}(\dot{\varepsilon}^{(n)})$ in the material coordinates of each layer of composite tows satisfy the condition of $I_1 \geq 1$ at the time step (n) and under load with strain rate $\dot{\varepsilon}$, failure occurs due to the tension in the fibers. $F_{1t}(\dot{\varepsilon}^{(n)})$, $F_6(\dot{\varepsilon}^{(n)})$ and $F_4(\dot{\varepsilon}^{(n)})$ are the rate-dependent longitudinal tensile, in-plane shear, and out-of-plane shear strength of the UD composite at time step (n). Experimental values reported in section 5.2.1.

3.1.2. Rate-dependent transverse tensile mode

"Transverse tensile mode" means traction failure perpendicular to the fiber direction of a tow. Rate-dependent transverse failure when subjected to transverse tensile stress $\sigma_{22}(\dot{\varepsilon}^{(n)}) > 0$, is predicted by

$$I_2 = \left(\frac{\sigma_{22}(\dot{\varepsilon}^{(n)})}{F_{2t}(\dot{\varepsilon}^{(n)})}\right)^2 + \left(\frac{\tau_{12}(\dot{\varepsilon}^{(n)})}{F_6(\dot{\varepsilon}^{(n)})}\right)^2 + \left(\frac{\tau_{23}(\dot{\varepsilon}^{(n)})}{F_4(\dot{\varepsilon}^{(n)})}\right)^2 \geq 1 \tag{36}$$

This equation states that when the stresses $\sigma_{22}(\dot{\varepsilon}^{(n)})$, $\tau_{12}(\dot{\varepsilon}^{(n)})$ and $\tau_{23}(\dot{\varepsilon}^{(n)})$ in the material coordinates of each layer of composite tows satisfy the condition of $I_2 \geq 1$ at the time step (n) and under load with strain rate $\dot{\varepsilon}$, failure occurs due to the transverse stresses in the matrix. $F_{2t}(\dot{\varepsilon}^{(n)})$ is rate-dependent transverse tensile strength of the UD composite at the time step (n).

Equations (35-36) are used for both composite tows and pure matrix (between tows). The strength values of composite tows, F_{1t}, F_{2t}, F_6, and F_4 at different strain rates are obtained through Eqs. (41-43). The strength values of matrix, $F_{1t}=F_{2t}$ and $F_4=F_6$ are obtained from Fig. 8 and Tables 5-6.

3.2. Strength values

The experimental results presented in section 5, illustrate that the tensile behavior of the WF laminate is primarily controlled by the fibrous composite tows along the load path, while the transverse composite tows fail due to matrix failure. The transverse damage occurs along the fiber direction without fiber breakage [23]. At the onset of failure of the WF composite under longitudinal tensile load, the longitudinal composite tows fail due to the tensile fiber failure and lost all load-carrying capacity. However, the transverse composite tows fail due to the transverse matrix cracking, but due to the friction between the fibers and the matrix, the tows do not lose their integrity and load-carrying capacity [24, 25]. The experimental data of the WF composite in section 5 demonstrates that during failure of the pure resin and transverse tows, which are prior to the failure of the longitudinal tows, there are no sudden steps in the stress-strain curves.

Some researchers have suggested that under transverse tension, the transverse modulus reduces to 0.01 of the initial values [26]. However, the onset of transverse failure is only a sign of first matrix cracking, which means that the composite is still capable of carrying more loading and the stiffness should not be reduced dramatically, but slowly [27].

In a WF composite, the longitudinal and transverse composite tows are bonded to each other by resin sub-elements. During matrix cracking of transverse tows and pure resin sub-elements, loss of strength does not occur dramatically but slowly. Therefore, in this work, the transverse modulus of the transverse tows and the modulus of pure resin are assumed to be $E_{dt+1} = d_f E_{dt}$, where d_f is the degradation factor. Its value ($d_f = 0.99$ in this work) is determined by try and error, *to adjust the predicted stress-strain curves to the experimental ones.* Such a high value means that the modulus reduction due to matrix cracking has a very small effect on the overall response of WF composite, perhaps due to the undegraded stiffness of the fiber tows. The final breaking point of the material is determined by the failure of the longitudinal tows, precipitating the failure of the WF laminate. The proposed damage propagation method is verified by the experimental results in the section 5.2.

Numerical predictions of the stress-strain curves calculated with six different number of increments are shown in Fig. 4. The maximum deviation from the experimental results is +1.3% for 110 increments and -5% for 300 increments. While low number of increments introduces a slight artificial stiffening, large number of increments have the opposite effect, inducing a slight artificial softening, but as it can be seen in the figure, the deviations are small.

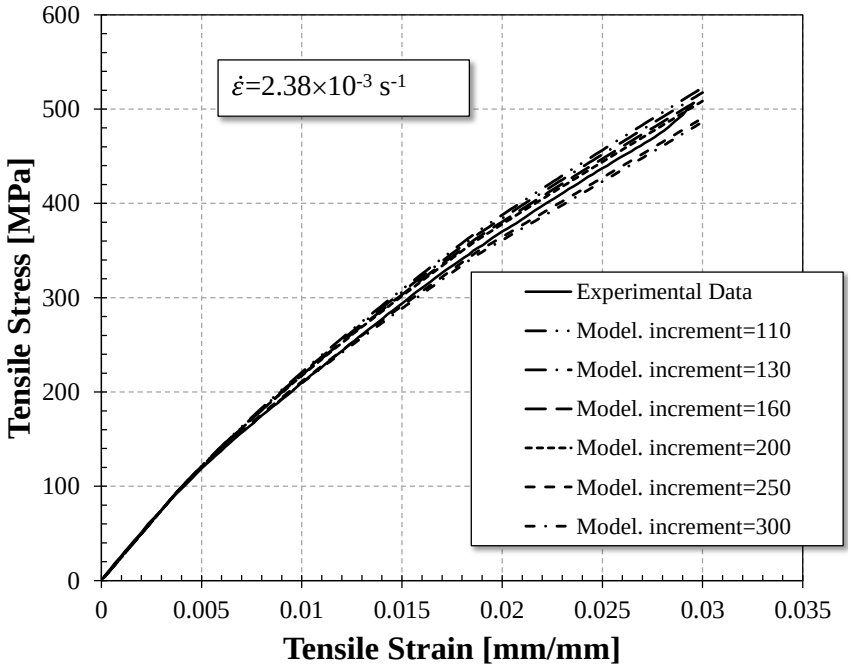

Fig. 4. Tensile stress-strain curves for different six number of increments

3.3. Flowchart of the MMS strength analysis

The flowchart of the MMS model is presented in Fig. 5. According to the applied strain rate on the composite tows, the share of strain rate of the polymeric matrix is determined, and the inelastic strain rate is calculated using Eq. (18). The stress-strain curve of the matrix is obtained and its tangent modulus at each time step can be calculated. It should be noted that at the first time-step, the calculation of the stiffness matrix of composite tows and matrix are based on the quasi-static strain rate. The updated value of tangent modulus of the matrix is used to update the bridging matrix in Eq. (2), which leads to update the compliance matrix of the composite tows and matrix sub-elements in Eq. (17). When the compliance matrix is updated, the local stiffness matrices in Eq. (30), and total stiffness matrices in Eq. (32) are updated. This means that an update of the value of tangent modulus of matrix material at each time step leads to an update of the mechanical properties of WF composite in Eq. (33).

At each small step, the tangent modulus from previous step is used as an input parameter, then its value is updated to achieve the convergency and used in the calculation of the stiffness matrices of the WF composite. The updated values of the stress in the sub-elements are checked in the failure criteria. If failure has been occurred, the relevant compliance matrix of the sub-element is reduced, Eq. (17), which reduces the local stiffness matrix, Eq. (30), and total stiffness matrices, Eq. (32). Otherwise, at the next time step, ε_{m+1}, the new stress value of polymeric matrix is calculated to update tangent modulus and stresses of the sub-elements. In Fig. 5, $I_k, k=1,2$ are different modes of failure. The tensile failure of composite tows along load direction, $I_1 \geq 1$, means the final failure of the WF composite.

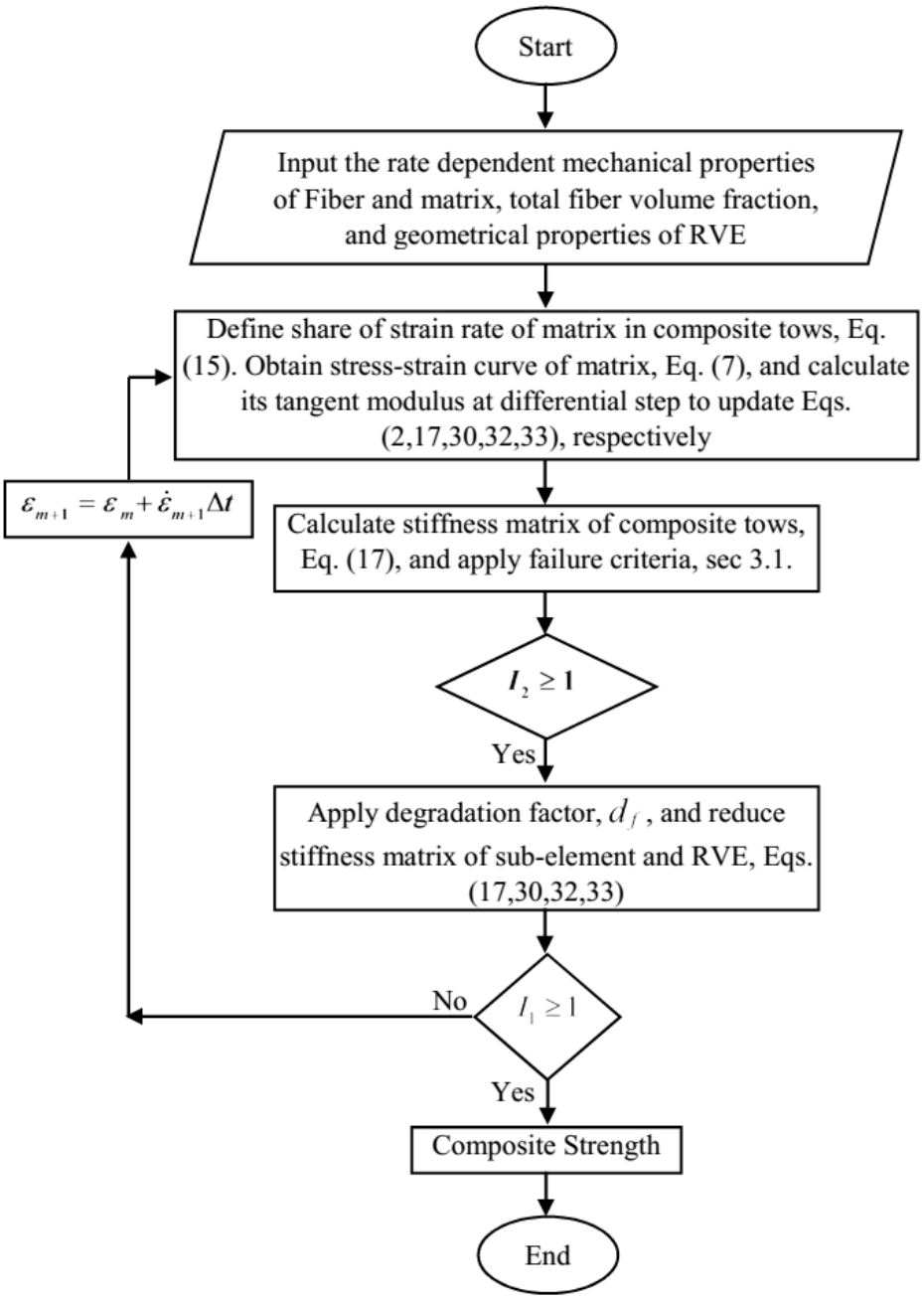

Fig. 5. Flowchart of the MMS model

4. Materials and methods

The MMS model requires the properties of its components under the rate-dependent loading to predict the behavior of the WF composite at various strain rates. In this study, the dynamic behavior of epoxy polymer as a matrix material and glass fibers are extracted using rate-dependent experiments on epoxy and UD glass/epoxy composites specimens. The experimental tests on the plain glass/epoxy WF composites are used to validate the MMS model. An Epolam

industrial epoxy resin was selected for the experimental part of this research, which includes Epolam resin 2017 and Hardener Epolam 2018. The physical properties and fabrication methods of tensile and shear specimens were described in the previous study [10]. The geometric specifications of the woven glass fabric are shown in Table 1.

Table 1. Geometrical specifications of woven glass fabric

Warp tow			Fill tow		
a_w (mm)	h_w (mm)	g_w (mm)	a_f (mm)	h_f (mm)	g_f (mm)
3.5	0.45	0.025	3.5	0.45	0.025

Six layers of reinforcements are selected to fabricate laminated UD and WF composites, which there is no relative change between the arrangements of the adjacent layers. The vacuum infusion process (VIP) is used to uniformly impregnate the layers and minimize cavities, poor or rich-resin regions, Fig. 6. It is noted that in the VIP, a black mesh is used. To reduce the porosity and voids of the WF composite to a minimum level, the mixed resin and hardener was degassed prior to the injection process. The properties of the UD and WF laminates are described in Table 2. The fiber volume fraction of laminates are calculated using matrix burn off method according to ASTM D3171 standard and reported in Table 2. Fiber properties are discussed in section 5.2.1.

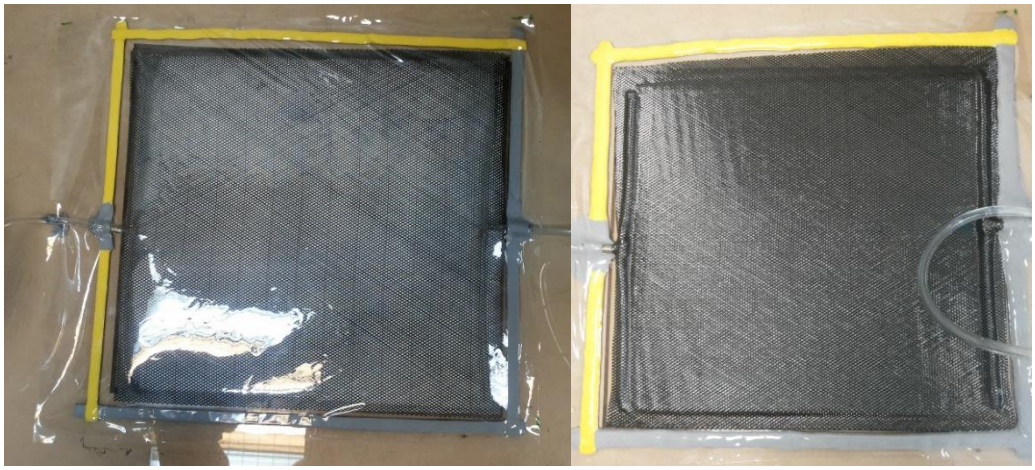

(a) (b)

Fig. 6. Photograph of the vacuum infusion process of WF laminate with black mesh

Table 2. Number of layers, thickness, and overall fiber volume fraction of manufactured laminates

Material	Code	Number of Layers	Laminate Thickness (mm)	Overall fiber volume fraction
WF Laminate	G-3	6	3.0	0.51
	G-4	6	2.7	0.59
UD laminate	UD	6	1.5	0.66

The mechanical behavior of the UD and WF composite are considered under rate-dependent tensile loadings, while the behavior of the epoxy polymer is considered under both rate-dependent tensile and shear loadings. Dimensions of specimens are listed in Table 3.

Table 3. Dimensions of specimens

	Material	
	WF and UD composite	Epoxy polymer
Tensile specimens	35×330 (mm)	35×250 (mm)
Shear specimens	-	75×70 (mm)

The WF and UD composites, and epoxy polymer specimens are tested at five different displacement rates, Table 4. It is noted that due to the different geometry of tensile and shear specimens, the different strain rates are induced in the specimens. The tensile and shear tests were performed using Instron 8802 in accordance with ASTM D3039 and ASTM D7078 standards.

Table 4. Applied displacement rates to samples

Material	Displacement rates
WF and UD composite	$2, 20, 200, 2000, 3240 \quad (mm/min)$
Epoxy polymer	$3, 30, 300, 2000, 3000 \quad (mm/min)$

In the proposed model, besides customary materials properties that can be measured by standard methods, there are only 3 parameters (α, β, and d_f). Parameters α and β are part of bridging matrix model, with values determined following the methodology explained in [6].

The value found for $d_f = 0.99$ (Section 3.2) suggests that matrix damage has negligible effect on the rate-dependent viscoplastic repose of WF composites subjected to in-plane traction loads. Thus, a set of experiments different from the validation ones was deemed unnecessary. Furthermore, testing equipment do not allow us to test other loading scenarios (besides uniaxial extension) under which more sophisticated, strain-dependent damage evolution laws may be needed.

5. Results and discussion

5.1. Experimental results

The viscoplastic model constants are characterized using several rate-dependent experimental tests on UD composite and epoxy polymer specimens, and to verify the MMS viscoplastic model, the rate-dependent experiments are carried out on the WF composite.

5.1.1. Stress-strain behavior of polymer matrix

In order to characterize and model the viscoplastic behavior of epoxy polymer based on Eq. (18), it is required to define tensile and shear tests at various strain rates. The epoxy polymer has tensile and shear gage of 130×35 mm and 25×70 mm with thickness of 5 mm, Fig. 7. The details of tensile and shear tests, and modeling the viscoplastic behavior of epoxy polymer are discussed in [10].

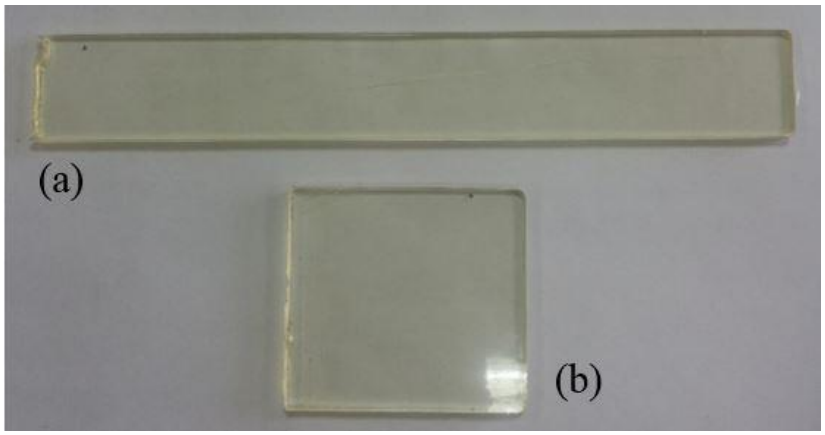

Fig. 7. Epoxy resin specimens for (a) tensile test, (b) shear test [10]

The experimental results of tensile and shear stress-strain curves at five strain rates are presented in Fig. 8 (a) and (b). The tensile stress-strain curves have slight curvature that repeated very well and ended with sudden fracture. At higher strain rates, the specimens show a lower curvature than at low strain rates, and the curve tends to be a straight line. Compared to tensile tests, a significant nonlinear stress-strain behavior is observed under shear loading even at low strain rate. The stress-strain curves at the end of the shear tests converge to a horizontal area before breaking point, this means that the saturation stress and shear strength of the material are convergent [10]. The values of the initial modulus, ultimate strength and failure strain for the tensile and shear loading are represented at different strain rates in Tables 5 and 6.

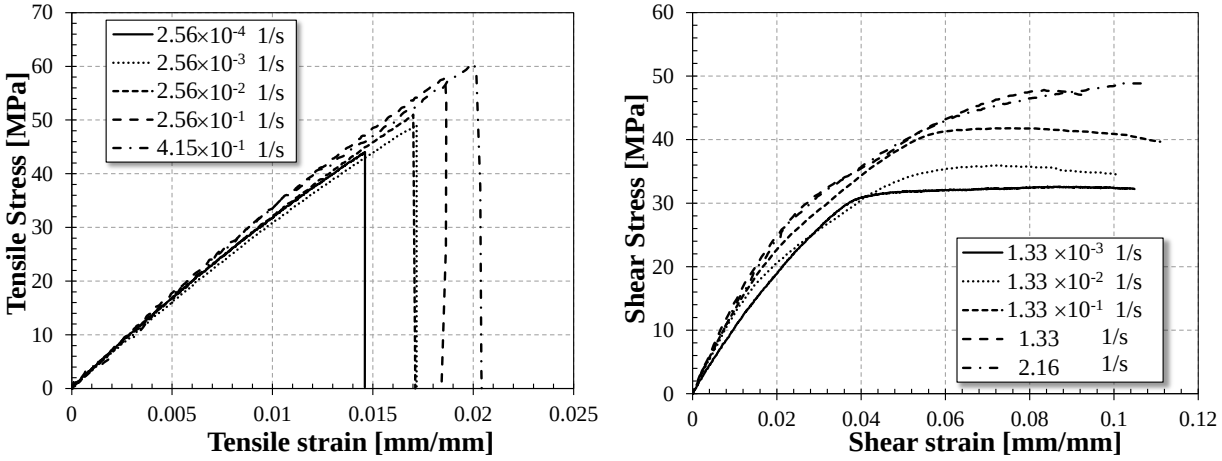

(a) (b)

Fig. 8. (a) Tensile tests, (b) shear tests of epoxy matrix performed at five strain rates [10]

Table 5. Experimental initial tensile modulus, tensile strength, and tensile strain-to-failure of epoxy matrix at five strain rates [10].

Strain rate [s^{-1}]	Initial modulus [GPa]	Ultimate Strength [MPa]	Failure strain
2.56×10^{-4}	3.20	44.1	0.015
2.56×10^{-3}	3.17	49.2	0.017
2.56×10^{-2}	3.28	51.0	0.017
2.56×10^{-1}	3.36	57.9	0.019
4.15×10^{-1}	3.39	60.5	0.021

Table 6. Experimental initial shear modulus, shear strength, and shear strain-to-failure of epoxy matrix at five strain rates [10].

Strain rate [s^{-1}]	Initial modulus [GPa]	Ultimate Strength [MPa]	Failure strain
1.33×10^{-3}	1.26	32.2	0.105
1.33×10^{-2}	1.29	35.9	0.100
1.33×10^{-1}	1.32	41.6	0.111
1.33	1.39	47.7	0.092
2.16	1.42	48.9	0.105

The strain was measured using the testing machine's built-in extensometer, and the compliance of testing machine used is much higher than the compliance of the specimens. The range of strain rate used for the testing and validations was aimed to characterize the mechanical properties at *some* strain rates and used them to predict the stress-strain curves at *some other* strain rates. Furthermore, the displacement rates were applied up to the maximum velocity limit of the testing machine, which is 3000 mm/min.

Fracture pattern of tensile specimen

The fracture patterns of tensile specimens at strain rates of 2.56×10^{-4} and 4.15×10^{-1} (s^{-1}) are shown in Figs. 9 (a) and (b) [10]. The fracture patterns show that the crack starts within the gauge length and propagates normal to the load direction. The fracture surfaces indicate that the specimens are sensitive to the normal stress and prove that the maximum average stress occurs within the gauge length rather than in the grips. These phenomena justify the application of rectangular specimens in accordance with ASTM D3039 standard.

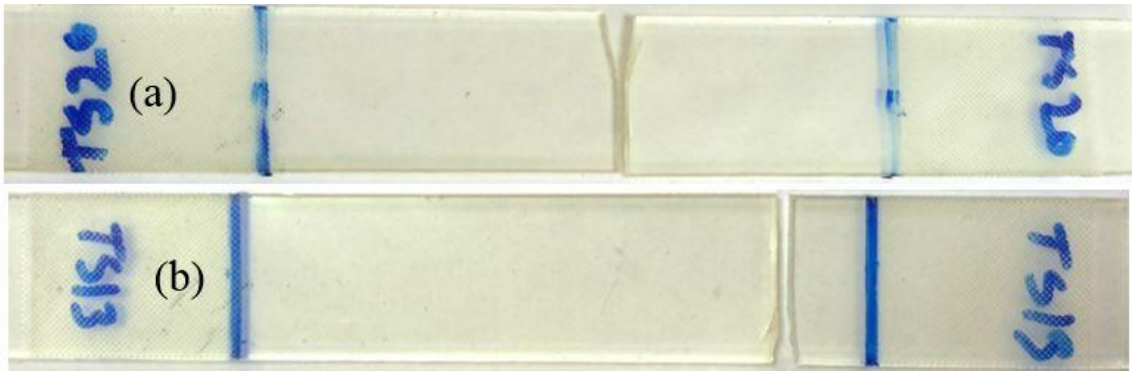

Fig. 9. Tensile-fracture patterns of resin specimens tested at (a) 2.56×10^{-4} 1/s and (b) 4.15×10^{-1} 1/s. [10]

Fracture pattern of shear specimen

The fracture patterns of shear specimens at strain rates of 1.33 and 1.33×10^{-1} (s^{-1}) are shown in Fig. 10 (a) and (b) [10]. Fracture patterns show that the fracture on the oblique plane about 45 degree starts from the middle of specimens and propagates toward the edge of specimen. The crack stops at the fixture and continues parallel to the fixtures to the two ends of the specimen. Further, the multi-crack in the oblique plane is due to the continuous loading after cracking.

(a) (b)

Fig. 10. Shear-Fracture patterns of resin specimens tested at (a) 1.33 1/s and (b) 0.133 1/s [10]

The strain-rate dependence of the moduli and strengths values of the tensile and shear tests are shown in Figs. 10 and 11 [10]. The global slope of the tensile stress-strain curve increases with increasing strain rate, so that the initial modulus and ultimate strength for increasing strain rate from $2.56\times10^{-4}\ s^{-1}$ to $4.15\times10^{-1}\ s^{-1}$, increase about 6.9% and 37.5%, Fig. 11 (a) and (b). The shear stress-strain curves show rate dependency, which over three decades of increasing strain rate from $1.33\times10^{-3}\ s^{-1}$ to $2.16\ s^{-1}$ the shear modulus and strength increase about 12% and 51.7%, Fig. 12 (a) and (b). The tensile and shear moduli have almost no scattering in experimental results, but the tensile and shear strengths have maximum scattering about 5% and 6% that are show by error bars.

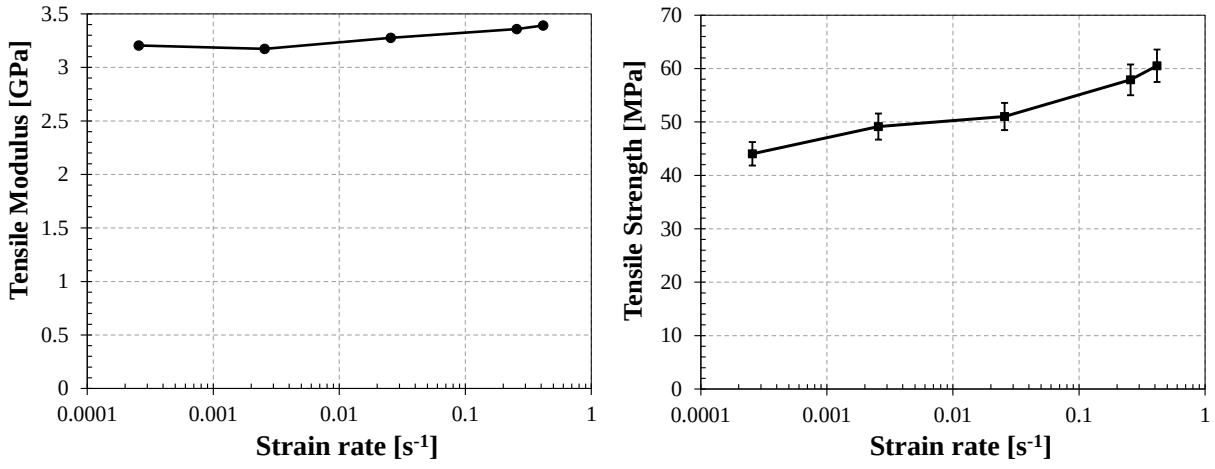

(a) (b)

Fig. 11. Rate dependency of the tensile (a) initial modulus and (b) strength of epoxy matrix [10].

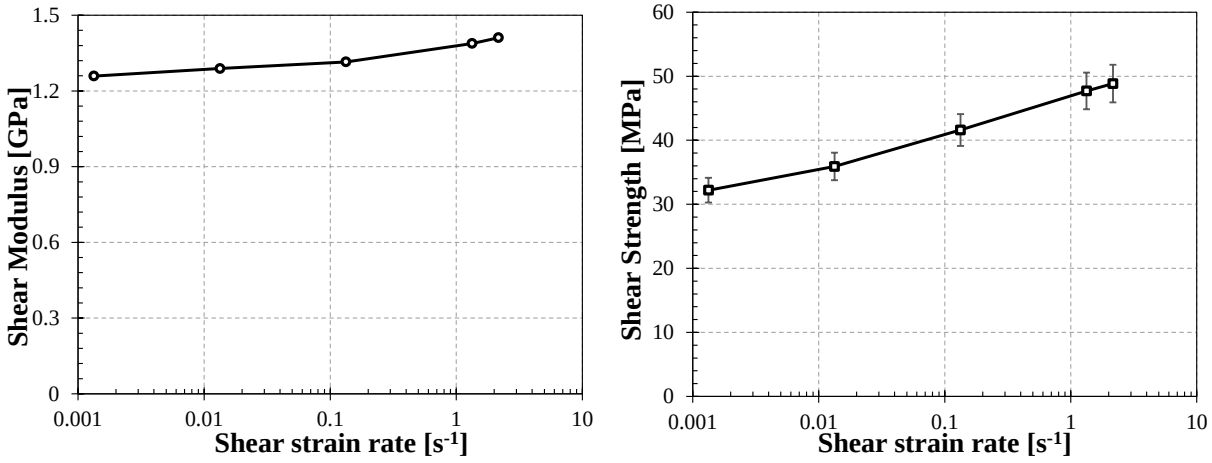

(a) (b)

Fig. 12. Rate dependency of the (a) shear initial Young's modulus and (b) shear strength of epoxy matrix [10]

5.1.2. Stress-strain behavior of UD composite

Study of the mechanical behavior of fibers as the reinforcement constituents of the composite under dynamic loadings show that some fibers, like carbon fibers, are not sensitive to the loading rate, but the mechanical properties of the glass fibers are function of the strain rate. The mechanical properties of fibers dominate the longitudinal mechanical properties of UD composite. Using rule of mixture method and knowing the fiber volume fraction, modulus and strength of the UD composite and matrix material, the strain-rate dependent mechanical properties of glass fibers are obtained. Then, a series of tensile tests at various strain rates are carried out on the UD glass/epoxy composite. The specimens of UD composite have a gage part of 25×210 mm, Fig. 13.

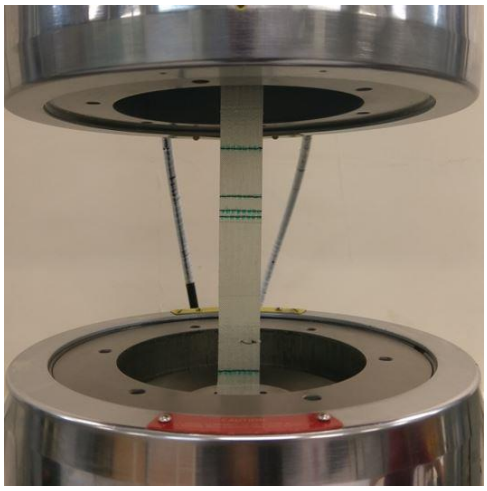

Fig. 13. UD composite specimen mounted on testing machine

The tensile stress-strain curves of UD composite at five strain rates are presented in Fig. 14. Due to the fiber dominant properties of the UD composite, the tensile stress-strain curves of the UD composite at different strain rates are nearly linear. The values of the initial modulus, ultimate strength and failure strain for the tensile loading are represented at different strain rates in Tables 7.

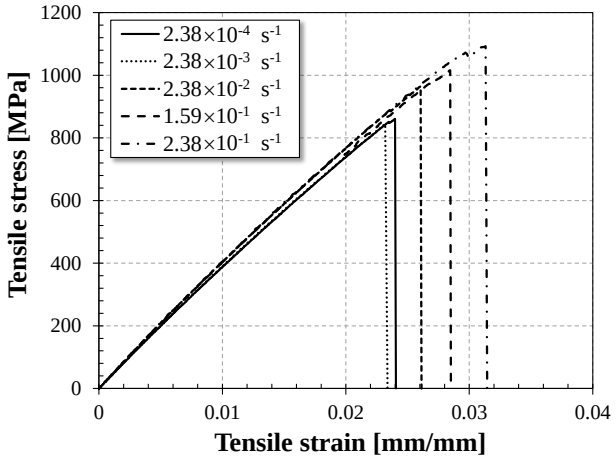

Fig. 14. Tensile stress-strain curves of UD composite at different strain rates

Table 7. Experimental results of initial modulus, strength, and failure strain of UD composite at five tensile strain rates

Strain rate [s^{-1}]	Initial modulus [GPa]	Ultimate Strength [MPa]	Failure strain
2.38×10^{-4}	39.8	827	0.024
2.38×10^{-3}	40.8	844	0.023
2.38×10^{-2}	41.7	964	0.026
1.59×10^{-1}	42.2	1016	0.029
2.38×10^{-1}	42.5	1092	0.031

The initial modulus and ultimate strength of UD glass/epoxy composite show rate-dependent behavior. Increasing strain rate from 2.38×10^{-4} to 2.38×10^{-1} s^{-1} cause increase about 5.8% and 32% in initial modulus and ultimate strength, Fig. 15 (a) and (b). The experimental scattering of the results of the modulus and strength are small about 3% that is negligible.

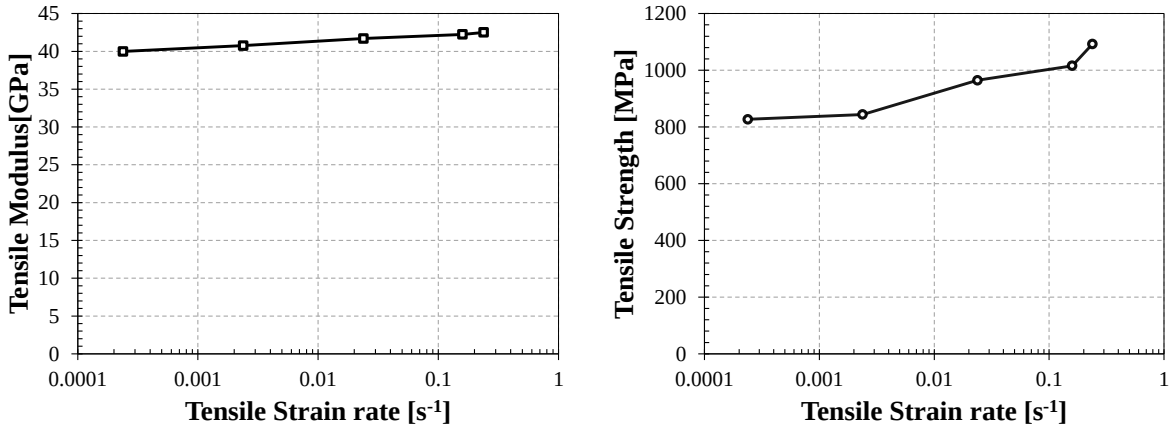

(a) (b)

Fig. 15. Rate dependency of the of UD composite (a) Initial modulus and (b) Ultimate tensile strength

5.1.3. Tensile stress-strain behavior of WF laminate

The gage length of the tensile test specimens of the WF glass/epoxy composite is 210 mm, Fig. 16. The specimens are tested at five strain rates from $2.38\times10^{-4}\ s^{-1}$ to $2.38\times10^{-1}\ s^{-1}$. Two WF laminates are used to perform all five strain rates, Table 2. Due to the difference in the fiber volume fraction of WF laminates, Table 8 shows which laminate was used for each strain rate. To ensure the repeatability of the results, each constant tensile strain rate was repeated three times. For instance, the tensile stress-strain curves at $1.59\times10^{-1}\ s^{-1}$ strain rate are presented in Fig. 17.

Table 8. Range of applied strain rate on each WF laminate

WF laminate Code	Applied strain rate (s^{-1})
G-1	$2.38\times10^{-4}, 2.38\times10^{-3}, 2.38\times10^{-2}$
G-7	$1.58\times10^{-1}, 2.38\times10^{-1}$

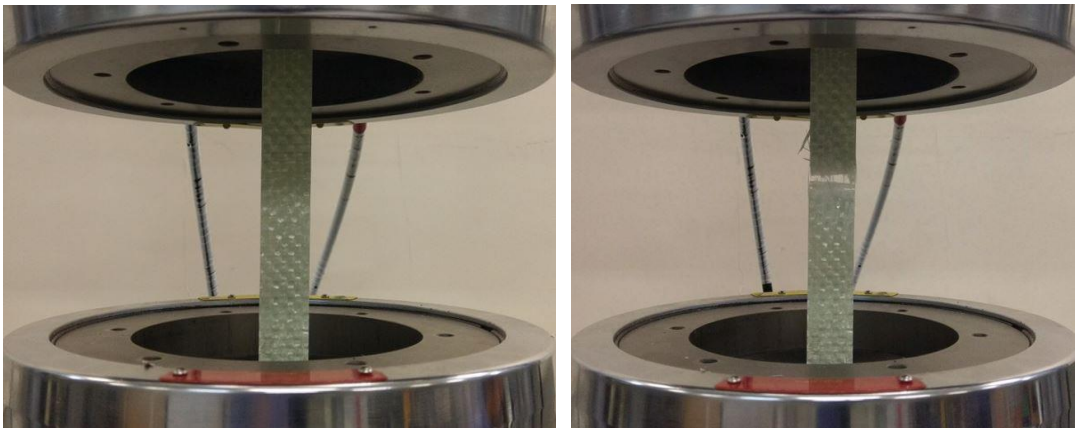

(a) (b)

Fig. 16. Tensile specimen of WF laminate. (a) Intact and (b) Failed specimen with $2.38\times10^{-2}\ s^{-1}$ strain rate

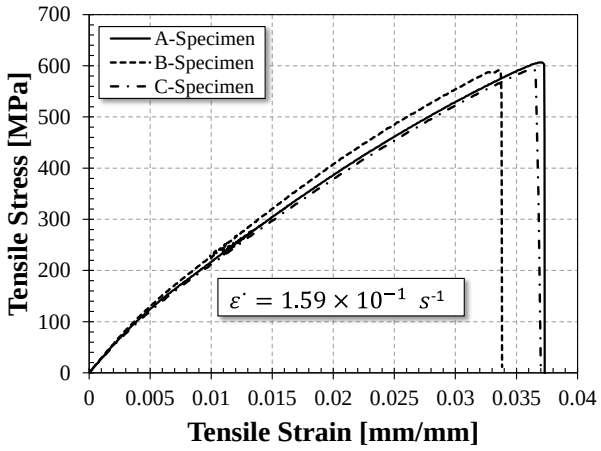

Fig. 17. Tensile stress-strain curves of WF laminate at $1.59\times10^{-1}\ s^{-1}$ strain rate.

It is observed that the initial modulus and the nonlinearity of the stress-strain curves are repeatable. The ultimate strength of the WF composite, i.e., the breaking point, has reasonable scattering. The longitudinal composite tows control the fracture of the WF composite. The pattern on the fracture surface, Fig. 16 (b), shows that the crack starts and grows at the mid-length of the gage length is normal to the load direction. The fracture of the transverse tows, with lower transverse strength, happens prior to the fiber rupture of the longitudinal tows that govern the ultimate strength.

Rate-dependency of the tensile modulus and strength

To study the rate-dependent behavior of the WF laminate under tensile loading, the tensile stress-strain curves are presented at five strain rates in Fig. 18. The curves start with small linear regions and with increasing strain, the curvature of curves that is the sign of nonlinearity increases. Two important parameters in the nonlinear behavior of material are the fabric pattern, and stiffness reduction due to the polymeric matrix plasticity and damage. The off-axis warp and

fill composite tows transition from linear to nonlinear behavior. The overall behavior of the WF composite under tensile load consists of linear fiber dominant behavior of longitudinal tows and nonlinear plastic behavior of the transverse tows, both with rate-dependent behavior. The values of the initial modulus, ultimate strength and failure strain for the tensile loading are represented at different strain rates in Table 9.

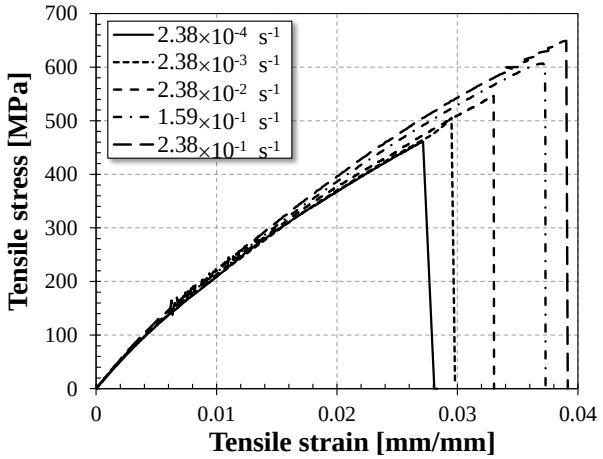

Fig. 18. Tensile stress-strain curves of WF laminate performed at five strain rates

Table 9. Experimental results of initial modulus, strength, and failure strain of the WF composite at five tensile strain rates

Strain rate [s^{-1}]	Initial modulus [GPa]	Ultimate Strength [MPa]	Failure strain
2.38×10^{-4}	25.04	460.7	0.027
2.38×10^{-3}	25.67	505.2	0.029
2.38×10^{-2}	26.21	546.4	0.033
1.59×10^{-1}	27.06	606.8	0.037
2.38×10^{-1}	28.15	649.2	0.039

To show the nonlinearity of the tensile stress-strain curves of the WF composite and their deviation from the linear behavior, a tangent line is drawn at the beginning of the curves, which representing the linear elastic behavior, and continues until the fracture strain. At each strain level, the degree of deviation from linear behavior is due to the local stiffness reduction for material and geometrical nonlinearity that lead to the reduction in stress level, Fig. 19. Tensile stress-strain curves have the same pattern. As the strain increases to the fracture point, at any constant strain rate, the nonlinearity increases dramatically. The continuous line in Fig. 19 represent the experimental results. The maximum deviation of tensile stress-strain curves from

the linear behavior occurs at fracture. Deviation for each strain rate are presented in Table 10. According to the results, the nonlinearity of the tensile stress-strain curves is significant.

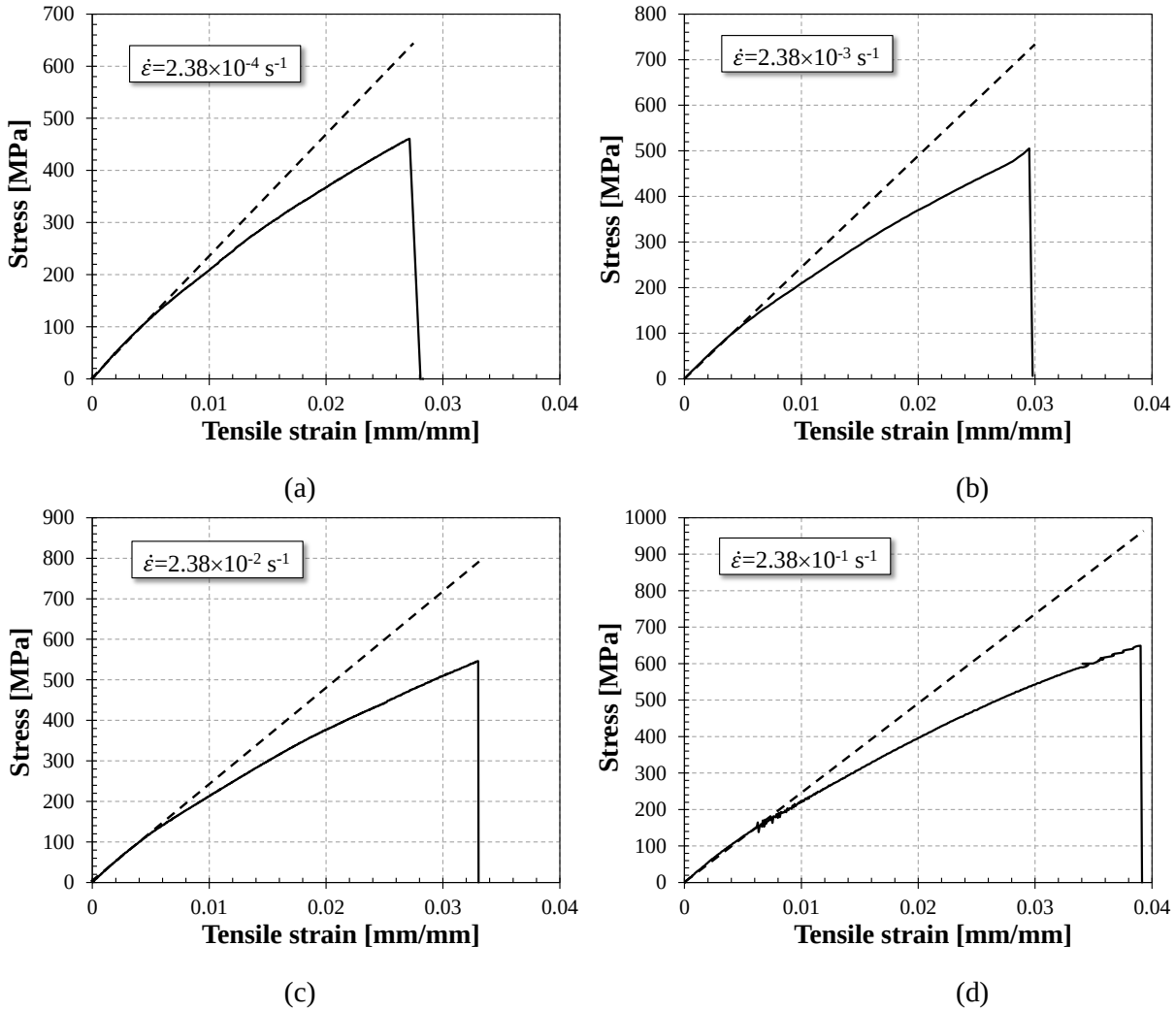

Fig. 19. Comparison of the maximum stress of the experimental results and linear pattern at different strain rates

Table 10. Comparison of experimental stress results and linear-pattern stress of the WF composite

Strain rate [s^{-1}]	Failure strain	Maximum experimental stress [MPa]	Maximum linear-pattern stress [MPa]	Deviation [%]
2.38×10^{-4}	0.027	461	640	39
2.38×10^{-3}	0.029	500	740	48
2.38×10^{-2}	0.033	546	800	46
2.38×10^{-1}	0.039	650	960	48

Two important parts of the tensile stress-strain curves are considered at different strain rates, the initial modulus and ultimate strength. Increasing strain rate from $2.38\times10^{-4}\ s^{-1}$ to $2.38\times10^{-1}\ s^{-1}$ increase initial modulus and ultimate strength about 12% and 40%, Fig. 20 (a) and (b). The scattering of the experimental results of the ultimate strength is about 5% that is shown by error bar, but for initial modulus is less that 3% that is ignorable.

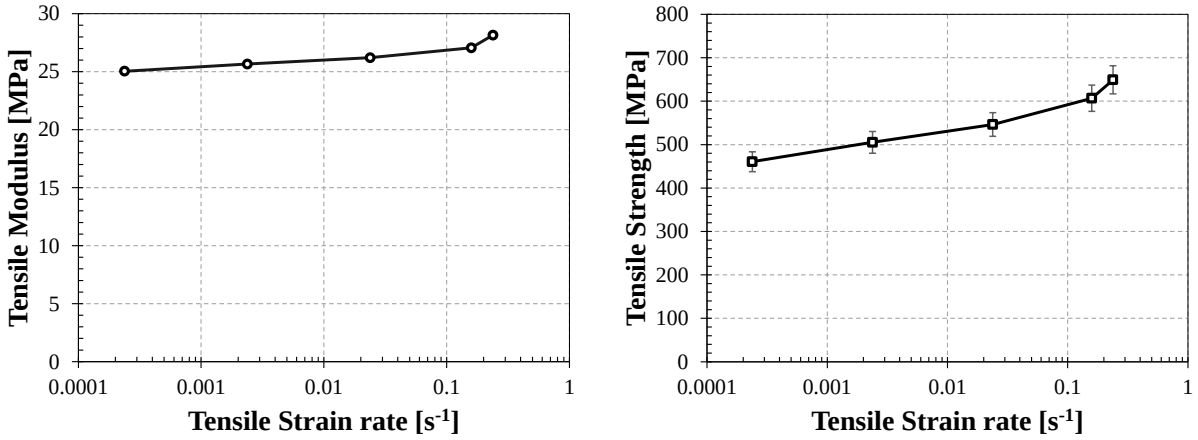

(a) (b)

Fig. 20. Rate-dependent behavior of (a) Initial modulus and (b) Ultimate strength of WF laminate

5.2. Model prediction results

5.2.1. Viscoplastic behavior of WF composite

The rate-dependent MMS model to predict the mechanical properties of the WF composites was presented in section 2, Eqs. (30)-(33). To apply this model, it is required to specify rate-dependent mechanical properties of fiber, matrix, and UD composites. The viscoplastic constitutive equation, Eq. (18), that is used to describe the viscoplastic behavior of the polymeric matrix has the following material constants [10], Table 11.

Table 11. Model parameters for the epoxy resin [10]

D_0 [s^{-1}]	Z_0 [MPa]	Z_1 [MPa]	n	q	C
10^6	627.2	1105.2	0.52	80.1	-1

Due to the rate-dependent behavior of the UD composite in Figs. 13 and 14, it is necessary to determine the mechanical properties of glass fibers at different strain rates. The longitudinal modulus of the UD composite follows the rule of mixture as

$$E_{11}(\dot{\varepsilon}) = v_f E_{11f}(\dot{\varepsilon}) + v_m E_{11m}(\dot{\varepsilon}) \tag{37}$$

where $E_{11}(\dot{\varepsilon})$, $E_{11f}(\dot{\varepsilon})$ and $E_{11m}(\dot{\varepsilon})$ are the longitudinal elastic modulus of the UD composite, fiber and matrix at strain rate $(\dot{\varepsilon})$, respectively. The fiber and matrix volume fractions are v_f and v_m. Similar to the rule of mixture for the longitudinal modulus of the UD composite, the following relation can be written for the rate-dependent longitudinal strength of UD composite $F_{1t}(\dot{\varepsilon})$ based on the longitudinal strength of fiber $F_{fa}(\dot{\varepsilon})$ and matrix $F_m(\dot{\varepsilon})$ at strain rate $(\dot{\varepsilon})$

$$F_{1t}(\dot{\varepsilon}) = v_f F_{fa}(\dot{\varepsilon}) + v_m F_m(\dot{\varepsilon}) \tag{38}$$

Using experimental results of the UD composite, Figs. 13 and 14, and relations (37) and (38), the elastic modulus and strength values of fiber at each strain rate are calculated. Using Eq. (34), the fitted equation for the elastic modulus $E_{fa}(\dot{\varepsilon}^f)$ and strength $F_{fa}(\dot{\varepsilon}^f)$ of the glass fiber in the following form are obtained

$$E_{fa}(\dot{\varepsilon}^f) = 55885[0.0019\ln(\frac{\dot{\varepsilon}^f}{2.38\times10^{-4}})+1] \quad (MPa) \quad \dot{\varepsilon}^f \geq 2.38\times10^{-4}\ (s^{-1}) \tag{39}$$

$$F_{fa}(\dot{\varepsilon}^f) = 1186.7[0.0464\ln(\frac{\dot{\varepsilon}^f}{2.38\times10^{-4}})+1] \quad (MPa) \quad \dot{\varepsilon}^f \geq 2.38\times10^{-4}\ (s^{-1}) \tag{40}$$

The value of shear modulus of glass fibers at different strain rate obtains from $E_{fa}(\dot{\varepsilon}^f) = 2G_{fa}(\dot{\varepsilon}^f)(1+\upsilon_f)$, where υ_f is Poisson's ratio of glass fibers that is 0.3. The fitted Eqs. (39) and (40) are presented in Fig. 21 (a) and (b).

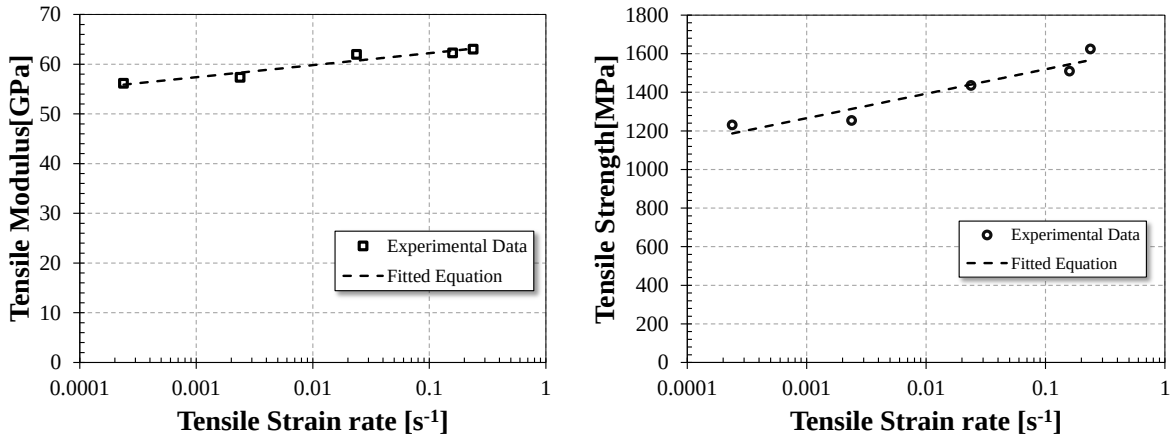

(a) (b)

Fig. 21. The fitted equations for the (a) modulus and (b) strength of the glass fiber at five strain rates

The model parameters α and β, Eq. (3), that are used to adjust the response of the UD composite tow to the experimental results are taken as 0.5 and 0.6, respectively. The values of M and N for discretization of the RVE, Fig. 3, are chosen as M=N=63. These values are increased in successive runs until convergence of predicted modulus and strength are achieved. No localization is detected because the domain coincides with the RVE, so that the response is periodic, which does not allow us to detect localization. The progressive damage model needs the strength of the UD composite at different strain rate, so that, the fitted Eq. (41) is used to describe the rate-dependent longitudinal strength of the UD composite $F_{1t}(\dot{\varepsilon})$. This fitted equation is presented in Fig. 22. The transverse and shear strengths of UD composite are estimated based on the $F_{1t}(\dot{\varepsilon})$ and results presented for UD glass/epoxy in [20]. The fitted equation for the transverse strength $F_{2t}(\dot{\varepsilon})$ and shear strength $F_6(\dot{\varepsilon})$ of the UD glass/epoxy composite are presented in Eqs. (42) and (43). It is observed that the transverse and shear strengths of the UD glass/epoxy are very close to the longitudinal and shear strengths of the epoxy matrix, Fig. 7.

$$F_{1t}(\dot{\varepsilon}) = 797.98[0.0465\ln(\frac{\dot{\varepsilon}}{2.38\times10^{-4}})+1] \quad (MPa) \quad \dot{\varepsilon} \geq 2.38\times10^{-4}\ (s^{-1}) \tag{41}$$

$$F_{2t}(\dot{\varepsilon}) = 47.673[0.0344\ln(\frac{\dot{\varepsilon}}{2\times10^{-3}})+1] \quad (MPa) \quad \dot{\varepsilon} \geq 2\times10^{-3}\ (s^{-1}) \tag{42}$$

$$F_6(\dot{\varepsilon}) = 39.42[0.0315\ln(\frac{\dot{\gamma}}{10^{-3}})+1] \quad (MPa) \quad \dot{\gamma} \geq 10^{-3}\ (s^{-1}) \tag{43}$$

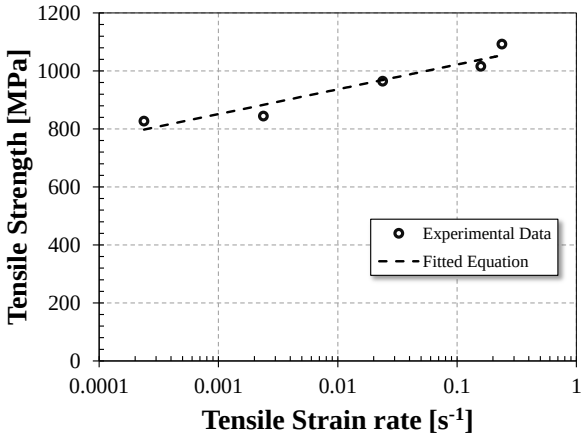

Fig. 22. The fitted equation of the longitudinal strength of the UD composite

Applying the material properties of the fibers and the matrix, the geometric description of the RVE, and the progressive damage model in the MMS model, the tensile behavior of the WF composite is predicted. Comparison of tensile stress-strain curves obtained from experimental results and predicted values of MMS model at different strain rates are presented in Fig. 23. The tensile stress-strain curves at different strain rates and the rate-dependency of the initial modulus

and ultimate strength are predicted well, Table 12. In addition to the viscoplasticity of the transverse composite tows, Eq. (17), the failure propagation method and selecting appropriate damage factor, section 3, reduce stiffness matrix properly and obtain stress-strain curve with acceptable curvature that follows the experimental results.

According to iso-stain hypothesis and continuity of strain over the WF composite, equal in-plane strains are applied in each element, Fig. 3, namely warp and fill composite tows and pure resin [15, 18, 21]. In each element of WF composite the warp and fill composite tows are under transverse and longitudinal tension. The transverse strength of composite tows and strength of pure resin are similar. However, due to the significant difference in their modulus, the pure resin undergoes degradation at a higher strain than the tows. Therefore, in terms of increasing strain along the fill direction, the warp tows, pure resin, and finally the fill tows are degraded. The tensile stress-strain curve displays some oscillatory behavior at the end of the simulation, when both the strain rate and the tensile strain at high, mainly in Fig. 19 (d) and barely noticeable in Fig. 18 (top curve).

At the applied strain rates in this study, the Poisson's ratio of the epoxy resin and glass fiber show no rate dependency. The experimental results on the UD glass/epoxy composite presented in this paper and those reported in [19] are of the same order of magnitude. The strain rate range used in this work is limited by the testing machine's limit speed of 3000 mm/min. Prediction and validation of this model at higher strain rates requires more capable equipment that is not available to us.

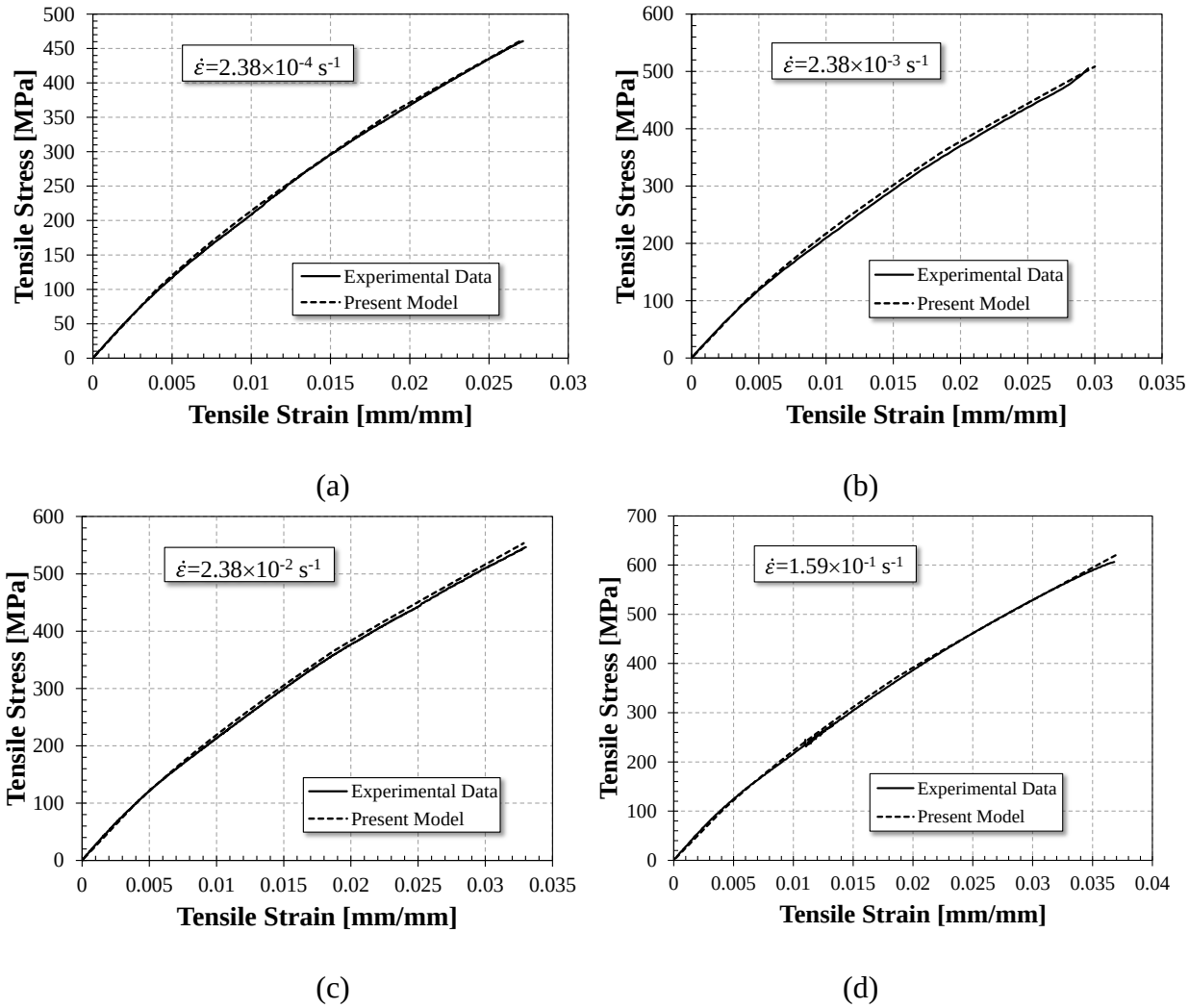

Fig. 23. Comparison of the present model and experimental results of the WF composite

Table 12. Comparison of experimental and predicted mechanical properties

	Initial modulus [GPa]			Ultimate strength [MPa]		
Strain rate (s^{-1})	Experimental	Prediction	Error [%]	Experimental	Prediction	Error [%]
2.38×10^{-4}	25.043	26.30	5.0	460.69	492.5	6.9
2.38×10^{-3}	25.661	26.49	3.2	505.21	541.0	7.1
2.38×10^{-2}	26.208	26.88	2.6	546.34	591.7	8.3
1.59×10^{-1}	27.059	27.36	1.1	606.75	665.6	9.7
2.38×10^{-1}	28.15	28.52	1.3	649.17	685.1	5.5

The fractured tensile specimens are presented in Fig. 24. Each specimen is related to a specific tensile strain rate. The crack initiation and propagation is normal to the load direction within the gage length. The fracture line is almost straight. There is no load eccentricity that creates bending moment in the specimens. The specimen of Fig. 24 (A) of strain rate 2.38×10^{-4} was painted with black color, and there are white spots over the surface of specimen. The white spots belong to the small cracks and matrix plasticity in the transverse composite tows that happened prior to the final failure. There is no significant damage in the transverse composite tows and they have not lost their strength with the initial failure. This proves the degradation method which indicates the modulus of the transverse composite tows should reduce gradually.

Fig. 24. Failed specimen of different tensile strain rates

5.2.2. Effects of out-of-plane stresses

Under tensile loading along the X direction, Figs. 1 and 2, the warp composite tows are subjected to the in-plane transverse tensile stress along the material coordinate 2_w, while the fill composite tows are subjected to the stress along the material coordinates 1_f, 3_f and 13_f. The model predicts that the presence of the normal and shear stresses in the direction of 3_f and 13_f should cause the separation of warp and fill composite tows and reduce the strength of the WF composite. The maximum of these stresses occur at the intersection of warp and fill tows where the fill undulation angle θ_f is maximum, Fig. 25. The predicted stress-strain curves related to the out-of-plane normal and shear stresses applied to the fill composite tow at different strain rates are presented in Fig. 26. It is observed that the out-of-plane stresses have sufficient values to create debonding between warp and fill tows and surpass the interface strength. Those values should increase with increasing strain rate. The interface strength is provided by the polymeric matrix material that has tensile and shear strength according to the Fig. 8 (a) and (b).

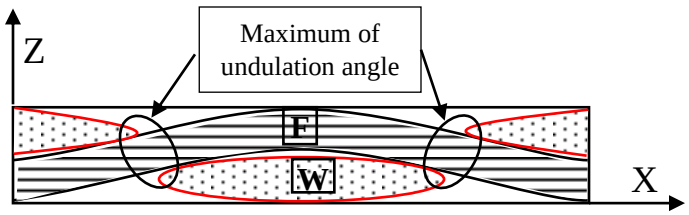

Fig. 25. Maximum of undulation angle in the fill tow

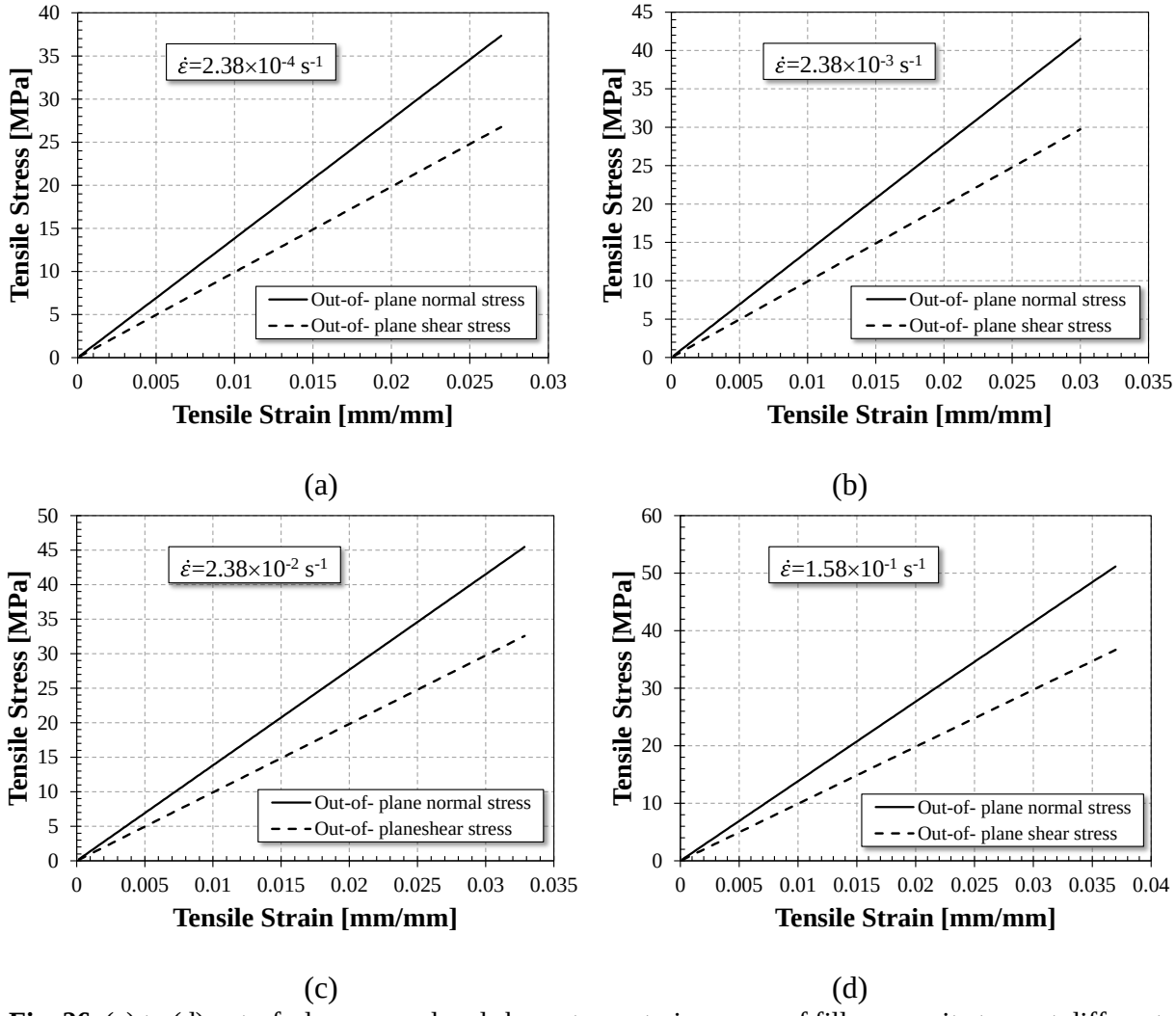

Fig. 26. (a) to (d) out-of-plane normal and shear stress-strain curves of fill composite tows at different strain rates

Transverse and out-of-plane shear stresses induced in the composite tows are calculated and included in the failure model, but according to the experimental observations in Fig. 24, there is no significant damage prior to the final failure of the longitudinal composite tows. It appears that under the conditions of this study, no significant fiber-matrix and tow-matrix interface debonding are apparent, and thus interface debonding is not included in the predictive model presented herein.

6. Conclusions

In the present study, a novel model with progressive damage model was developed to analyze the nonlinear rate-dependent behavior of the WF composite. A micro-meso-scale (MMS) model was developed to predict the rate-dependent behavior of the WF composite, and to consider nonlinearity of the WF composite due to the undulated geometry and nonlinear material behavior. The viscoelastic fiber and viscoplastic matrix were combined to create UD composite tow with viscoplastic behavior. The micro-scale model determined the effect of rate-dependency in the fiber and matrix, and nonlinearity of the matrix on the viscoplastic behavior of composite tows. Furthermore, with implementation of the geometrical characteristics and stacking sequence of the composite tows in the meso-scale model, a WF composite with anisotropic viscoplastic behavior was concluded. At each differential step, the viscoplasticity of the matrix and viscoelasticity of the fiber were updated, and subsequently, the viscoplasticity of the composite tows and the WF composite were updated.

A strain-rate-dependent progressive damage model was developed to assess the effect of matrix cracking on the prediction of the stress-strain curves of the WF composite. The progressive damage model detected the onset of failure in the sub-elements and reduced their relevant stiffness matrices. Then, the stiffness matrices of the element and RVE were updated and the applied load was redistributed over the undamaged regions. A series of the experimental tests were performed at various strain-rate on the polymer matrix and UD composite to derive the viscoplastic model constants. To verify the MMS model, tensile tests at different strain-rates were carried out on the WF composite. Based on the analytical and experimental investigations, the following observations are noted:

- The initial modulus and ultimate strength values as predicted by the MMS model at various strain rates were in line with experimental results.

- The MMS model predicts the nonlinearity of the experimental stress-strain curves at various strain rates by considering the effects of the material and geometrical properties in the micro- and meso-scale model.

- The rate-dependency of the WF composite is due to the different rate-dependency of the fiber and matrix. Their behavior and load-share are integrated in the micro-scale model. The resultant rate-dependency viscoplastic composite tows are integrated in the meso-scale model.

- The nonlinearity of the WF composite is due to the nonlinear behavior of the matrix, the geometrical features of the woven fabric, and the potential damage that may occur in the micro- and meso-scale models.

- The experimental results of the fracture patterns of the WF composites show that there is no significant damage in the transverse composite tows prior to the final fracture. The damage is smoothly propagated over the specimens and leads to a fracture plane in the middle of the specimens, perpendicular to the load direction.

- The proposed model can be implemented in a finite element framework.

CRediT authorship contribution statement

Ehsan Shafiei: Conceptualization; Methodology; Resources; Investigation; Data curation; Data validation; Writing original draft. **Mahdi Saed Kiasat**: Supervision. **Ever J. Barbero**: review & editing.

Acknowledgement

This research did not receive any specific grant from funding agencies in the public, commercial, or not-for-profit sectors.

References

[1] K. Chung , H. Ryou, Development of viscoelastic/rate-sensitive-plastic constitutive law for fiber-reinforced composites and its applications. Part I: Theory and material characterization, Composites science and technology. 69 (2009) 284-291
[2] S. Ogihara , K. L. Reifsnider, Characterization of nonlinear behavior in woven composite laminates, Applied composite materials. 9 (2002) 249-263
[3] S. V. Thiruppukuzhi , C. Sun, Models for the strain-rate-dependent behavior of polymer composites, Composites science and technology. 61 (2001) 1-12
[4] S. Marguet, P. Rozycki , L. Gornet, A rate dependent constitutive model for carbon-fiber reinforced plastic woven fabrics, Mechanics of Advanced Materials and Structures. 14 (2007) 619-631
[5] C. Hochard, P.-A. Aubourg , J.-P. Charles, Modelling of the mechanical behaviour of woven-fabric CFRP laminates up to failure, Composites science and technology. 61 (2001) 221-230
[6] Z. ming Huang, The mechanical properties of composites reinforced with woven and braided fabrics, Composites science and technology. 60 (2000) 479-498
[7] X. Bai, M. A. Bessa, A. R. Melro, P. P. Camanho, L. Guo , W. K. Liu, High-fidelity micro-scale modeling of the thermo-visco-plastic behavior of carbon fiber polymer matrix composites, Composite Structures. 134 (2015) 132-141
[8] R. K. Goldberg , D. C. Stouffer, Strain rate dependent analysis of a polymer matrix composite utilizing a micromechanics approach, Journal of Composite Materials. 36 (2002) 773-793
[9] S.-Y. Hsu, T. Vogler , S. Kyriakides, Inelastic behavior of an AS4/PEEK composite under combined transverse compressionand shear. Part II: modeling, International Journal of Plasticity. 15 (1999) 807-836
[10] E. Shafiei , M. S. Kiasat, A new viscoplastic model and experimental characterization for thermosetting resins, Polymer Testing. 84 (2020) 106389
[11] J. Lu, P. Zhu, Q. Ji , Z. Cheng, Experimental study of in-plane mechanical properties of carbon fibre woven composite at different strain rates, Polymers and Polymer Composites. 25 (2017) 289-298

[12] X. Li, Y. Yan, L. Guo , C. Xu, Effect of strain rate on the mechanical properties of carbon/epoxy composites under quasi-static and dynamic loadings, Polymer Testing. 52 (2016) 254-264
[13] X. Chen, Y. Li, Z. Zhi, Y. Guo , N. Ouyang, The compressive and tensile behavior of a 0/90 C fiber woven composite at high strain rates, Carbon. 61 (2013) 97-104
[14] J. Fitoussi, F. Meraghni, Z. Jendli, G. Hug , D. Baptiste, Experimental methodology for high strain-rates tensile behaviour analysis of polymer matrix composites, Composites science and technology. 65 (2005) 2174-2188
[15] A. Adumitroaie , E. J. Barbero, Stiffness and strength prediction for plain weave textile reinforced composites, Mechanics of Advanced Materials and Structures. 19 (2012) 169-183
[16] Y. Kwon , W. Cho, Multilevel, micromechanical model for thermal analysis of woven-fabric composite materials, Journal of Thermal Stresses. 27 (2004) 59-73
[17] D. Scida, Z. Aboura, M. Benzeggagh , E. Bocherens, Prediction of the elastic behaviour of hybrid and non-hybrid woven composites, Composites science and technology. 57 (1998) 1727-1740
[18] E. J. Barbero, Introduction to composite materials design,3rd ed, CRC press.(2017).
[19] H. T. Hahn , S. W. Tsai, Introduction to composite materials, CRC Press.(1980).
[20] M. M. Shokrieh, R. Mosalmani , M. J. Omidi, Strain-rate dependent micromechanical method to investigate the strength properties of glass/epoxy composites, Composite Structures. 111 (2014) 232-239
[21] S. Z. Sheng , S. Van Hoa, Three dimensional micro-mechanical modeling of woven fabric composites, Journal of Composite Materials. 35 (2001) 1701-1729
[22] K. I. Tserpes, G. Labeas, P. Papanikos , T. Kermanidis, Strength prediction of bolted joints in graphite/epoxy composite laminates, Composites Part B: Engineering. 33 (2002) 521-529
[23] N. K. Naik, P. Yernamma, N. M. Thoram, R. Gadipatri , V. R. Kavala, High strain rate tensile behavior of woven fabric E-glass/epoxy composite, Polymer Testing. 29 (2010) 14-22
[24] G. Belingardi, H. Mehdipour, E. Mangino , B. Martorana, Progressive damage analysis of a rate-dependent hybrid composite beam, Composite Structures. 154 (2016) 433-442
[25] R. O'higgins, C. McCarthy , M. McCarthy, Identification of damage and plasticity parameters for continuum damage mechanics modelling of carbon and glass fibre-reinforced composite materials, Strain. 47 (2011) 105-115
[26] D. Blackketter, D. Walrath , A. Hansen, Modeling damage in a plain weave fabric-reinforced composite material, Journal of Composites, Technology and Research. 15 (1993) 136-142
[27] E. J. Barbero , F. Cosso, Determination of material parameters for discrete damage mechanics analysis of carbon-epoxy laminates, Composites Part B: Engineering. 56 (2014) 638-646